EPJ manuscript No.
(will be inserted by the editor)

Study of multi-muon events produced in $p\bar{p}$ collisions at $\sqrt{s} = 1.96$ TeV

T. Aaltonen[22], J. Adelman[12], B. Álvarez González[10], S. Amerio[40,41], D. Amidei[33], A. Anastassov[36], J. Antos[13], G. Apollinari[16], A. Apresyan[48], T. Arisawa[54], A. Artikov[14], W. Ashmanskas[16], P. Azzurri[43,46], W. Badgett[16], B.A. Barnett[24], V. Bartsch[30], D. Beecher[30], S. Behari[24], G. Bellettini[43,44], D. Benjamin[15], D. Bisello[40,41], I. Bizjak[30,l], C. Blocker[7], B. Blumenfeld[24], A. Bocci[15], V. Boisvert[49], G. Bolla[48], D. Bortoletto[48], J. Boudreau[47], A. Bridgeman[23], L. Brigliadori[40], C. Bromberg[34], E. Brubaker[12], J. Budagov[14], H.S. Budd[49], S. Budd[23], S. Burke[16], K. Burkett[16], G. Busetto[40,41], P. Bussey[20,e], K. L. Byrum[2], S. Cabrera[15,k], C. Calancha[31], M. Campanelli[34], F. Canelli[16], B. Carls[23], R. Carosi[43], S. Carrillo[17,g], B. Casal[10], M. Casarsa[16], A. Castro[5,6], P. Catastini[43,45], D. Cauz[51,52], V. Cavaliere[43,45], S.H. Chang[25,26,27,28,29], Y.C. Chen[1], M. Chertok[8], G. Chiarelli[43], G. Chlachidze[16], K. Cho[25,26,27,28,29], D. Chokheli[14], J.P. Chou[21], K. Chung[11], Y.S. Chung[49], C.I. Ciobanu[42], M.A. Ciocci[43,45], A. Clark[19], D. Clark[7], G. Compostella[40], M.E. Convery[16], J. Conway[8], M. Cordelli[18], G. Cortiana[40,41], C.A. Cox[8], D.J. Cox[8], F. Crescioli[43,44], C. Cuenca Almenar[8,k], J. Cuevas[10,j], J.C. Cully[33], D. Dagenhart[16], M. Datta[16], T. Davies[20], P. de Barbaro[49], M. Dell'Orso[43,44], L. Demortier[50], J. Deng[15], M. Deninno[5], G.P. di Giovanni[42], B. Di Ruzza[51,52], J.R. Dittmann[4], S. Donati[43,44], J. Donini[40], T. Dorigo[40], J. Efron[37], R. Erbacher[8], D. Errede[23], S. Errede[23], R. Eusebi[16], W.T. Fedorko[12], J.P. Fernandez[31], R. Field[17], G. Flanagan[48], R. Forrest[8], M.J. Frank[4], M. Franklin[21], J.C. Freeman[16], I. Furic[17], M. Gallinaro[50], J. Galyardt[11], F. Garberson[9], J.E. Garcia[19], A.F. Garfinkel[48], K. Genser[16], H. Gerberich[23], D. Gerdes[33], V. Giakoumopoulou[3], P. Giannetti[43], K. Gibson[47], J.L. Gimmell[49], C.M. Ginsburg[16], N. Giokaris[3], M. Giordani[51,52], P. Giromini[18], G. Giurgiu[24], V. Glagolev[14], D. Glenzinski[16], N. Goldschmidt[17], A. Golossanov[16], G. Gomez[10], M. Goncharov[32], O. González[31], I. Gorelov[21], A.T. Goshaw[15], K. Goulianos[50], A. Gresele[40,41], S. Grinstein[21], J. Guimaraes da Costa[21], Z. Gunay-Unalan[34], K. Hahn[32], S.R. Hahn[16], B.-Y. Han[49], J.Y. Han[49], F. Happacher[18], M. Hare[53], R.M. Harris[16], M. Hartz[47], K. Hatakeyama[50], S. Hewamanage[4], D. Hidas[15], C.S. Hill[9,b], A. Hocker[16], S. Hou[1], R.E. Hughes[37], J. Huston[34], J. Incandela[9], A. Ivanov[8], E.J. Jeon[25,26,27,28,29], M.K. Jha[5], S. Jindariani[16], W. Johnson[8], M. Jones[48], K.K. Joo[25,26,27,28,29], S.Y. Jun[11], J.E. Jung[25,26,27,28,29], D. Kar[17], Y. Kato[39], B. Kilminster[16], D.H. Kim[25,26,27,28,29], H.S. Kim[25,26,27,28,29], H.W. Kim[25,26,27,28,29], J.E. Kim[25,26,27,28,29], M.J. Kim[18], S.B. Kim[25,26,27,28,29], Y.K. Kim[12], L. Kirsch[7], S. Klimenko[17], B. Knuteson[32], B.R. Ko[15], D.J. Kong[25,26,27,28,29], J. Konigsberg[17], A. Korytov[17], D. Krop[12], N. Krumnack[4], M. Kruse[15], V. Krutelyov[9], N.P. Kulkarni[55], Y. Kusakabe[54], S. Kwang[12], A.T. Laasanen[48], S. Lami[43], R.L. Lander[8], K. Lannon[37,i], G. Latino[43,45], I. Lazzizzera[40,41], H.S. Lee[12], S. Leone[43], M. Lindgren[16], A. Lister[8], D.O. Litvintsev[16], M. Loreti[40,41], L. Lovas[13], D. Lucchesi[40,41], P. Lukens[16], G. Lungu[50], R. Lysak[13], R. Madrak[16], K. Maeshima[16], K. Makhoul[32], T. Maki[22], P. Maksimovic[24], A. Manousakis-Katsikakis[3], F. Margaroli[48], C.P. Marino[23], V. Martin[20,f], R. Martínez-Ballarín[31], M. Mathis[24], P. Mazzanti[5], P. Mehtala[22], P. Merkel[48], C. Mesropian[50], T. Miao[16], N. Miladinovic[7], R. Miller[34], C. Mills[21], A. Mitra[1], G. Mitselmakher[17], N. Moggi[5], C.S. Moon[25,26,27,28,29], R. Moore[16], A. Mukherjee[16], R. Mumford[24], M. Mussini[5,6], J. Nachtman[16], I. Nakano[38], A. Napier[53], V. Necula[15], O. Norniella[23], E. Nurse[30], S.H. Oh[15], Y.D. Oh[25,26,27,28,29], I. Oksuzian[17], T. Okusawa[39], R. Orava[22], S. Pagan Griso[40,41], E. Palencia[16], V. Papadimitriou[16], A.A. Paramonov[12], B. Parks[37], G. Pauletta[51,52], M. Paulini[11], D.E. Pellett[8], A. Penzo[51], T.J. Phillips[15], G. Piacentino[43], L. Pinera[17], K. Pitts[23], O. Poukhov[14,†], F. Prakoshyn[14], A. Pronko[16], F. Ptohos[16,d], E. Pueschel[11], A. Rahaman[47], N. Ranjan[48], I. Redondo[31], V. Rekovic[35], F. Rimondi[5,6], A. Robson[20], T. Rodrigo[10], E. Rogers[23], S. Rolli[53], R. Roser[16], M. Rossi[51], R. Rossin[9], A. Ruiz[10], J. Russ[11], V. Rusu[16], W.K. Sakumoto[49], L. Santi[51,52], K. Sato[16], A. Savoy-Navarro[42], P. Schlabach[16], E.E. Schmidt[16], M.A. Schmidt[12], M. Schmitt[36], T. Schwarz[8], L. Scodellaro[10], A. Sedov[48], S. Seidel[35], Y. Seiya[39], A. Semenov[14], L. Sexton-Kennedy[16], F. Sforza[43], A. Sfyrla[23], S.Z. Shalhout[55], S. Shiraishi[12], M. Shochet[12], A. Sidoti[43], A. Sisakyan[14], A.J. Slaughter[16], J. Slaunwhite[37], K. Sliwa[53], J.R. Smith[8], A. Soha[8], V. Sorin[34], P. Squillacioti[43,45], R. St. Denis[20], D. Stentz[36], J. Strologas[35], G.L. Strycker[33], J.S. Suh[25,26,27,28,29], A. Sukhanov[17], I. Suslov[14], R. Takashima[38], R. Tanaka[38], M. Tecchio[33], P.K. Teng[1] K. Terashi[50], J. Thom[16,c], A.S. Thompson[20], G.A. Thompson[23], P. Ttito-Guzmán[31], S. Tokar[13], K. Tollefson[34], S. Torre[18], D. Torretta[16], P. Totaro[51,52], S. Tourneur[42], M. Trovato[43], S.-Y. Tsai[1], S. Vallecorsa[19], N. van Remortel[22,a], A. Varganov[33], E. Vataga[43,46], F. Vázquez[17,g] G. Velev[16], C. Vellidis[3], V. Veszpremi[48], M. Vidal[31], R. Vidal[16], I. Vila[10], R. Vilar[10], T. Vine[30], M. Vogel[35], G. Volpi[43,44], R.G. Wagner[2], R.L. Wagner[16], T. Wakisaka[39], S.M. Wang[1], B. Whitehouse[53], E. Wicklund[16], S. Wilbur[12], P. Wittich[16,c], S. Wolbers[16], C. Wolfe[12], T. Wright[33], X. Wu[19], K. Yamamoto[39], U.K. Yang[12,h], Y.C. Yang[25,26,27,28,29], K. Yorita[12], T. Yoshida[39], G.B. Yu[49], I. Yu[25,26,27,28,29], S.S. Yu[16], J.C. Yun[16],

A. Zanetti[51], X. Zhang[23], S. Zucchelli[5,6],

(CDF Collaboration)

[1] Institute of Physics, Academia Sinica, Taipei, Taiwan 11529, Republic of China
[2] Argonne National Laboratory, Argonne, Illinois 60439, USA
[3] University of Athens, 157 71 Athens, Greece
[4] Baylor University, Waco, Texas 76798, USA
[5] Istituto Nazionale di Fisica Nucleare Bologna, I-40127 Bologna, Italy
[6] Istituto Nazionale di Fisica Nucleare Bologna, [w]University of Bologna, I-40127 Bologna, Italy
[7] Brandeis University, Waltham, Massachusetts 02254, USA
[8] University of California, Davis, Davis, California 95616, USA
[9] University of California, Santa Barbara, Santa Barbara, California 93106, USA
[10] Instituto de Fisica de Cantabria, CSIC-University of Cantabria, 39005 Santander, Spain
[11] Carnegie Mellon University, Pittsburgh, PA 15213, USA
[12] Enrico Fermi Institute, University of Chicago, Chicago, Illinois 60637, USA
[13] Comenius University, 842 48 Bratislava, Slovakia; Institute of Experimental Physics, 040 01 Kosice, Slovakia
[14] Joint Institute for Nuclear Research, RU-141980 Dubna, Russia
[15] Duke University, Durham, North Carolina 27708, USA
[16] Fermi National Accelerator Laboratory, Batavia, Illinois 60510, USA
[17] University of Florida, Gainesville, Florida 32611, USA
[18] Laboratori Nazionali di Frascati, Istituto Nazionale di Fisica Nucleare, I-00044 Frascati, Italy
[19] University of Geneva, CH-1211 Geneva 4, Switzerland
[20] Glasgow University, Glasgow G12 8QQ, United Kingdom
[21] Harvard University, Cambridge, Massachusetts 02138, USA
[22] Division of High Energy Physics, Department of Physics, University of Helsinki and Helsinki Institute of Physics, FIN-00014, Helsinki, Finland
[23] University of Illinois, Urbana, Illinois 61801, USA
[24] The Johns Hopkins University, Baltimore, Maryland 21218, USA
[25] Center for High Energy Physics: Kyungpook National University, Daegu 702-701, Korea
[26] Seoul National University, Seoul 151-742, Korea
[27] Sungkyunkwan University, Suwon 440-746, Korea
[28] Korea Institute of Science and Technology Information, Daejeon, 305-806, Korea
[29] Chonnam National University, Gwangju, 500-757, Korea
[30] University College London, London WC1E 6BT, United Kingdom
[31] Centro de Investigaciones Energeticas Medioambientales y Tecnologicas, E-28040 Madrid, Spain
[32] Massachusetts Institute of Technology, Cambridge, Massachusetts 02139, USA
[33] University of Michigan, Ann Arbor, Michigan 48109, USA
[34] Michigan State University, East Lansing, Michigan 48824, USA
[35] University of New Mexico, Albuquerque, New Mexico 87131, USA
[36] Northwestern University, Evanston, Illinois 60208, USA
[37] The Ohio State University, Columbus, Ohio 43210, USA
[38] Okayama University, Okayama 700-8530, Japan
[39] Osaka City University, Osaka 588, Japan
[40] Istituto Nazionale di Fisica Nucleare, Sezione di Padova-Trento, I-35131 Padova, Italy
[41] Istituto Nazionale di Fisica Nucleare, University of Padova, I-35131 Padova, Italy
[42] LPNHE, Universite Pierre et Marie Curie/IN2P3-CNRS, UMR7585, Paris, F-75252 France
[43] Istituto Nazionale di Fisica Nucleare Pisa, I-56127 Pisa, Italy
[44] Istituto Nazionale di Fisica Nucleare Pisa, University of Pisa, I-56127 Pisa, Italy
[45] Istituto Nazionale di Fisica Nucleare Pisa, University of Siena, I-56127 Pisa, Italy
[46] Istituto Nazionale di Fisica Nucleare Pisa, Scuola Normale Superiore, I-56127 Pisa, Italy
[47] University of Pittsburgh, Pittsburgh, Pennsylvania 15260, USA
[48] Purdue University, West Lafayette, Indiana 47907, USA
[49] University of Rochester, Rochester, New York 14627, USA
[50] The Rockefeller University, New York, New York 10021, USA
[51] Istituto Nazionale di Fisica Nucleare Trieste/Udine, 34100 Trieste, Italy
[52] University of Trieste/Udine, 33100 Udine, Italy
[53] Tufts University, Medford, Massachusetts 02155, USA
[54] Waseda University, Tokyo 169, Japan
[55] Wayne State University, Detroit, Michigan 48201, USA

the date of receipt and acceptance should be inserted later

Abstract. We report a study of multi-muon events produced at the Fermilab Tevatron collider and recorded by the CDF II detector. In a data set acquired with a dedicated dimuon trigger and corresponding to an integrated luminosity of 2100 pb^{-1}, we isolate a significant sample of events in which at least one of the muon candidates is produced outside of the beam pipe of radius 1.5 cm. The production cross section and kinematics of events in which both muon candidates are produced inside the beam pipe are successfully modeled by known QCD processes which include heavy flavor production. In contrast, we are presently unable to fully account for the number and properties of the remaining events, in which at least one muon candidate is produced outside of the beam pipe, in terms of the same understanding of the CDF II detector, trigger, and event reconstruction. Several topological and kinematic properties of these events are presented in this paper. These events offer a plausible resolution to long-standing inconsistencies related to $b\bar{b}$ production and decay.

† Deceased
[a] Visitor from Universiteit Antwerpen, B-2610 Antwerp, Belgium
[b] Visitor from University of Bristol, Bristol BS8 1TL, United Kingdom
[c] Visitor from Cornell University, Ithaca, NY 14853, USA
[d] Visitor from University of Cyprus, Nicosia CY-1678, Cyprus
[e] Visitor from Royal Society of Edinburgh/Scottish Executive Support Research Fellow
[f] Visitor from University of Edinburgh, Edinburgh EH9 3JZ, United Kingdom
[g] Visitor from Universidad Iberoamericana, Mexico D.F., Mexico
[h] Visitor from University of Manchester, Manchester M13 9PL, England
[i] Visitor from University of Notre Dame, Notre Dame, IN 46556, USA
[j] Visitor from University de Oviedo, E-33007 Oviedo, Spain
[k] Visitor from IFIC(CSIC-Universitat de Valencia), 46071 Valencia, Spain
[l] On leave from J. Stefan Institute, Ljubljana, Slovenia

1 Introduction

This study was motivated by the presence of several inconsistencies that affect or affected measurements of the $b\bar{b}$ production at the Tevatron: (a) the ratio of the observed $b\bar{b}$ correlated production cross section to the exact next-to-leading-order (NLO) QCD prediction [1] is measured to be $R = 1.15 \pm 0.21$ when b quarks are selected via secondary vertex identification, whereas this ratio is found to be significantly larger than two when identifying b quarks through their semileptonic decays [2]; (b) sequential semileptonic decays of single b quarks are supposedly the main source of dileptons with invariant mass smaller than that of b quarks, but the observed invariant mass spectrum is not well modeled by the simulation of this process [3]; and (c) the value of $\bar{\chi}$, the average time-integrated mixing probability of b flavored hadrons, derived from the ratio of muon pairs from semileptonic decays of b and $\bar{b}$ quarks with same and opposite sign charge, is measured at hadron colliders to be significantly larger than that measured by the LEP experiments [4,5].

The first inconsistency (a) has been addressed in a recent study of the CDF collaboration [6]. That study uses a data sample acquired with a dedicated dimuon trigger to re-measure the correlated $\sigma_{b\to\mu,\bar{b}\to\mu}$ cross section. As in previous studies [4,7], Ref. [6] makes use of the precision tracking provided by the CDF silicon microvertex detector to evaluate the fractions of muons due to the decays of long-lived b- and c-hadrons, and to the other background contributions. The new measurement is in good agreement with theoretical expectations ($R = 1.20 \pm 0.21$), as well as with analogous measurements that identify b quarks via secondary vertex identification. However, it is also substantially smaller than previous measurements of this cross section [7,8]. The new CDF measurement [6] requires that both trigger muons arise from particles that have decayed inside the beam pipe of 1.5 cm radius. According to the simulation, approximately 96% of the known sources of dimuons, such as Drell-Yan, Υ, Z^0, and heavy flavor production, satisfy this condition. We will show that not only the rate, but also the kinematic properties of the events that satisfy this condition are correctly modeled by the simulation of known processes. This article also identifies a large sample of events that does not satisfy this condition. This component, which was present but not accounted for in previous measurements in which this decay-radius requirement was not made, will be described and investigated at length in this article. Although we cannot fully explain this component in terms of known sources, the identification of this type of event provides a plausible resolution to the set of inconsistencies mentioned at the beginning of this section.

We utilize the same dimuon data set, simulated samples, and analysis tools described in Ref. [6]. Section 2 describes the detector systems relevant to this analysis. The data selection and Monte Carlo simulation are briefly summarized in Sec. 3. Section 4 investigates differences in the experimental methods used to derive $\sigma_{b\to\mu,\bar{b}\to\mu}$ in Ref. [6] and in previous measurements, and isolates a large sample of events in which at least one muon candidate is produced beyond the beam pipe. Section 5 connects the presence of these events to the discrepancy between the observed and predicted invariant mass spectrum of lepton pairs produced by single b quark sequential decays. The properties of these events are explored in Secs. 6 and 7. Our conclusions are summarized in Sec. 8.

2 CDF II detector and trigger

CDF II is a multipurpose detector, equipped with a charged particle spectrometer and a finely segmented calorimeter. In this section, we describe the detector components that are relevant to this analysis. The description of these subsystems can be found in Refs. [9–18]. Two devices inside the 1.4 T solenoid are used for measuring the momentum of charged particles: the silicon vertex detector (SVXII and ISL) and the central tracking chamber (COT). The SVXII detector consists of microstrip sensors arranged in six cylindrical shells with radii between 1.5 and 10.6 cm, and with a total z coverage [1] of 90 cm. The first SVXII layer, also referred to as the L00 detector, is made

[1] In the CDF coordinate system, θ and ϕ are the polar and azimuthal angles of a track, respectively, defined with respect to the proton beam direction, z. The pseudorapidity η is defined as $-\ln\,\tan(\theta/2)$. The transverse momentum of a particle is $p_T = p\,\sin(\theta)$. The rapidity is defined as $y = 1/2 \cdot \ln((E+p_z)/(E-p_z))$, where E and p_z are the energy and longitudinal momentum of the particle associated with the track.

of single-sided sensors mounted on the beryllium beam pipe. The remaining five SVXII layers are made of double-sided sensors and are divided into three contiguous five-layer sections along the beam direction z. The vertex z-distribution for $p\bar{p}$ collisions is approximately described by a Gaussian function with a rms of 28 cm. The transverse profile of the Tevatron beam is circular and has a rms spread of $\simeq 25$ μm in the horizontal and vertical directions. The SVXII single-hit resolution is approximately 11 μm and allows a track impact parameter [2] resolution of approximately 35 μm, when also including the effect of the beam transverse size. The two additional silicon layers of the ISL help to link tracks in the COT to hits in the SVXII. The COT is a cylindrical drift chamber containing 96 sense wire layers grouped into eight alternating superlayers of axial and stereo wires. Its active volume covers $|z| \leq 155$ cm and 40 to 140 cm in radius. The transverse momentum resolution of tracks reconstructed using COT hits is $\sigma(p_T)/p_T^2 \simeq 0.0017$ $[\mathrm{GeV}/c]^{-1}$. The trajectory of COT tracks is extrapolated into the SVXII detector, and tracks are refitted with additional silicon hits consistent with the track extrapolation.

The central muon detector (CMU) is located around the central electromagnetic and hadronic calorimeters, which have a thickness of 5.5 interaction lengths at normal incidence. The CMU detector covers a nominal pseudorapidity range $|\eta| \leq 0.63$ relative to the center of the detector, and is segmented into two barrels of 24 modules, each covering 15° in ϕ. Every module is further segmented into three submodules, each covering 4.2° in ϕ and consisting of four layers of drift chambers. The smallest drift unit, called a stack, covers a 1.2° angle in ϕ. Adjacent pairs of stacks are combined together into a tower. A track segment (hits in two out of four layers of a stack) detected in a tower is referred to as a CMU stub. A second set of muon drift chambers (CMP) is located behind an additional steel absorber of 3.3 interaction lengths. The chambers are 640 cm long and are arranged axially to form a box around the central detector. The CMP detector covers a nominal pseudorapidity range $|\eta| \leq 0.54$ relative to the center of the detector. Muons which produce a stub in both the CMU and CMP systems are called CMUP muons. The CMX muon detector consists of eight drift chamber layers and scintillation counters positioned behind the hadron calorimeter. The CMX detector extends the muon coverage to $|\eta| \leq 1$ relative to the center of the detector.

The luminosity is measured using gaseous Cherenkov counters (CLC) that monitor the rate of inelastic $p\bar{p}$ collisions. The inelastic $p\bar{p}$ cross section at $\sqrt{s} = 1960$ GeV is scaled from measurements at $\sqrt{s} = 1800$ GeV using the calculations in Ref. [19]. The integrated luminosity is determined with a 6% systematic uncertainty [20].

CDF uses a three-level trigger system. At Level 1 (L1), data from every beam crossing are stored in a pipeline capable of buffering data from 42 beam crossings. The L1 trigger either rejects events or copies them into one of the four Level 2 (L2) buffers. Events that pass the L1 and L2 selection criteria are sent to the Level 3 (L3) trigger, a cluster of computers running speed-optimized reconstruction code.

For this study, we select events with two muon candidates identified by the L1 and L2 triggers. The L1 trigger uses tracks with $p_T \geq 1.5$ GeV/c found by a fast track processor (XFT). The XFT examines COT hits from the four axial superlayers and provides $r-\phi$ information in azimuthal sections of 1.25°. The XFT passes the track information to a set of extrapolation units that determine the CMU towers in which a CMU stub should be found if the track is a muon. If a stub is found, a L1 CMU primitive is generated. The L1 dimuon trigger requires at least two CMU primitives, separated by at least two CMU towers. The L2 trigger additionally requires that at least one of the muons also has a CMP stub matched to an XFT track with $p_T \geq 3$ GeV/c. All these trigger requirements are emulated by the detector simulation on a run-by-run basis. The L3 trigger requires a pair of CMUP muons with invariant mass larger than 5 GeV/c^2, and $|\delta z_0| \leq 5$ cm, where z_0 is the z coordinate of the muon track at its point of closest approach to the beam line in the $r-\phi$ plane. These requirements define the dimuon trigger used in this analysis.

Two other triggers are also utilized to acquire calibration samples used in this analysis. We use events acquired requiring a L1 CMUP primitive with $p_T \geq 4$ GeV/c accompanied by a L2 requirement of an additional track with $p_T \geq 2$ GeV/c and impact parameter $0.12 \leq d \leq 1$ mm as measured by the Silicon Vertex Trigger (SVT) [21]. The SVT calculates the impact parameter of each XFT track, with respect to the beam line, with a 50 μm resolution that includes the 25 μm contribution of the beam transverse width. Events selected with this trigger, referred to as $\mu-$SVT, are used to verify the muon detector acceptance and the muon reconstruction efficiency. We use an additional trigger, referred to as CHARM, that acquires events with two SVT tracks with $p_T \geq 2$ GeV/c and with impact parameter $0.12 \leq d \leq 1.00$ mm. In this data sample, we reconstruct $D^0 \to K^-\pi^+$ decays to measure the probability that the punchthrough of a charged hadron mimics a muon signal.

3 Data selection and Monte Carlo simulations

This study starts using the same data set and analysis selection criteria employed in the measurement of the correlated $b\bar{b}$ cross section [6], that corresponds to an integrated luminosity of 742 pb^{-1}. When extending our study to the smaller subsets of events containing multi muons, we will use larger data sets corresponding to integrated luminosities of 1426 and 2100 pb^{-1}. The correlated $b\bar{b}$ cross section measurement selects events acquired with the dimuon trigger and which contain at least two CMUP muons with same or opposite sign charge. If events contain more than two muons that pass the trigger requirements and analysis selection, the two with the highest transverse momenta are considered as trigger (or primary)

[2] The impact parameter d is the distance of closest approach of a track to the primary event vertex in the transverse plane.

muons. Events are reconstructed offline taking advantage of more refined calibration constants and reconstruction algorithms than those used by the L3 trigger. COT tracks are extrapolated into the SVXII detector, and refitted adding hits consistent with the track extrapolation. Stubs reconstructed in the CMU and CMP detectors are matched to tracks with $p_T \geq 3$ GeV/c. A track is identified as a CMUP muon if $\Delta r\phi$, the distance in the $r-\phi$ plane between the track projected to the CMU (CMP) chambers and a CMU (CMP) stub, is less than 30 (40) cm. We require that muon-candidate stubs correspond to a L1 CMU primitive, and correct the muon momentum for energy losses in the detector. We also require the z_0 distance between two muon candidates to be smaller than 1.5 cm. We reconstruct primary vertices using all tracks with SVXII hits that are consistent with originating from a common vertex. In events in which more than one interaction vertex has been reconstructed, we use the one closest in z to the average of the muon track z_0-positions and within a 6 cm distance. We evaluate the impact parameter of each muon track with respect to the primary vertex. The primary vertex coordinates transverse to the beam direction are measured with an accuracy of approximately 3 μm [6]. Cosmic rays are removed by requiring that the azimuthal angle between muons with opposite charge is smaller than 3.135 radians. Muon pairs arising from cascade decays of a single b quark are removed by selecting dimuon candidates with invariant mass greater than 5 GeV/c^2. We also reject muon pairs with invariant mass larger than 80 GeV/c^2 that are mostly contributed by Z^0 decays. The data sample that survives these selection criteria consists of 743006 events.

In this study, data are compared to different simulated samples. The heavy flavor production is simulated with the HERWIG Monte Carlo program [22], the settings of which are described in Appendix A of Ref. [6]. Hadrons with heavy flavors are subsequently decayed using the EVTGEN Monte Carlo program [23]. The detector response to particles produced by the above generators is modeled with the CDF II detector simulation that in turn is based on the GEANT Monte Carlo program [24].

4 Study of the data sample composition

The procedure to extract $\sigma_{b\to\mu,\bar{b}\to\mu}$ from the data is to fit the observed impact parameter distributions of the selected muon pairs with the expected impact parameter distributions of muons from various sources. The dominant sources of reconstructed muons are believed to be semileptonic decays of bottom and charmed hadrons, prompt decays of quarkonia, Drell-Yan production, and muons mimicked by prompt hadrons or hadrons arising from heavy flavor decays [3]. In the following, the sum of these contributions will be referred to as prompt plus heavy flavor (P+HF) production. Monte Carlo simulations are used to model the impact parameter distributions of muons from b- and c-hadron decays. The impact parameter distribution of muons from prompt sources, such as quarkonia decays and Drell-Yan production, is constructed using muons from $\Upsilon(1S)$ decays. To ensure an accurate impact parameter measurement, analyses performed by the CDF collaboration customarily require that each muon track is reconstructed using silicon hits in at least three out of the eight layers of the SVXII and ISL detectors (referred to as standard SVX selection in the following). However, in order to properly model the data with the templates of the different P+HF contributions mentioned above, Ref. [6] has used stricter selection criteria, referred to as tight SVX selection in the following, by requiring muon tracks with hits in the first two layers of the SVXII detector, and at least in two of the remaining four outer layers.

Table 1. Number of events attributed to the different dimuon sources by the fit to the muon impact-parameter distribution in the range $0-0.2$ cm. The fit parameters BB, CC, and PP represent the $b\bar{b}$, $c\bar{c}$, and prompt dimuon contributions, respectively. The component BC represents events containing b and c quarks. The fit parameter BP (CP) estimates the number of events in which there is only one b (c) quark in the detector acceptance and the second muon is produced by prompt hadrons in the recoiling light jet that mimick a muon signal. The data correspond to an integrated luminosity of 742 pb^{-1}.

Component	No. of Events
BB	54583 ± 678
CC	24458 ± 1565
PP	41556 ± 651
BP	10598 ± 744
CP	10024 ± 1308
BC	2165 ± 693

The tight SVX requirements reduce the data sample to 143743 events. The sample composition determined by the fit is shown in Table 1. The projection of the two-dimensional impact parameter distribution is compared to the fit result in Fig. 1. After removing the small contribution of muons mimicked by hadrons from heavy flavor decays, the study in Ref. [6] determines the size of $b\bar{b}$ production to be 52400 ± 2747 events. For muons with $p_T \geq 3$ GeV/c and $|\eta| \leq 0.7$, Ref. [6] reports $\sigma_{b\to\mu,\bar{b}\to\mu} = 1549 \pm 133$ pb. The ratio of this cross section to the NLO prediction (1.20 ± 0.21) is appreciably smaller than that reported in previous measurements [7,8], and in agreement with what obtained with secondary vertex identification (1.15 ± 0.21) [26,27]. This result mitigates previous inconsistencies between measurements and theoretical predictions of the correlated $b\bar{b}$ cross section.

However, since the shape of the impact parameter templates for the various P+HF components does not depend on the type (standard or tight) of SVX selection, a new problem arises that concerns the data sample composition prior to any SVX requirements. The tight SVX require-

[3] We follow the methodology pionereed in previous measurements. For example, muon tracks from pion and kaon in-flight-decays inside the tracking volume are regarded as prompt tracks because the track reconstruction algorithms are believed to remove decay muons with large kinks.

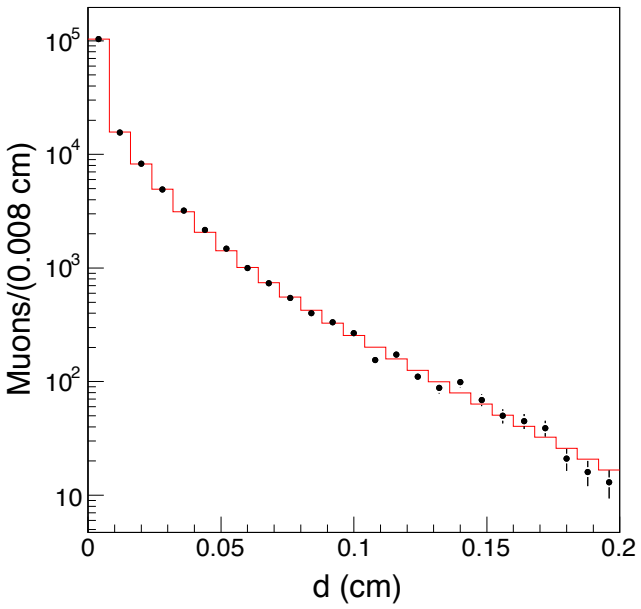

Fig. 1. The projection of the two-dimensional impact parameter distribution of muon pairs onto one of the two axes is compared to the fit result (histogram).

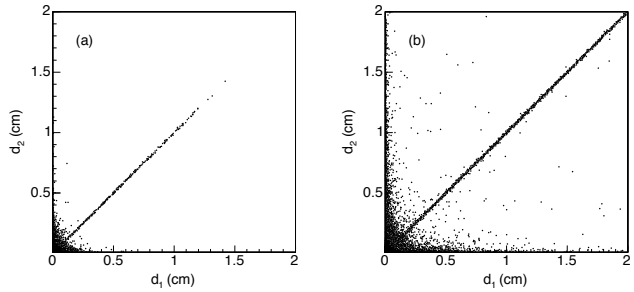

Fig. 2. Two-dimensional impact parameter distributions of muons that pass the (a) tight and (b) standard SVX requirements. Cosmic muons are reconstructed as two back-to-back muons of opposite charge and cluster along the $d_1 = d_2$ diagonal.

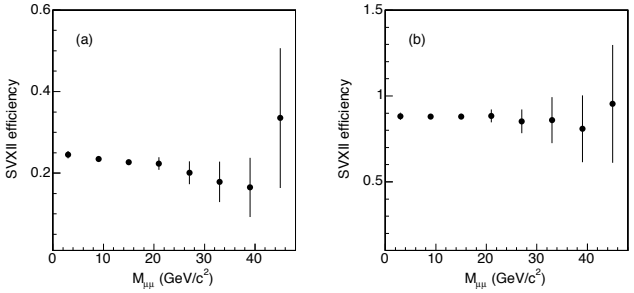

Fig. 3. Efficiency of SVX tight (a) and standard (b) selection in simulated dimuon events due to heavy flavor production (see text). The efficiency is shown as a function of the dimuon invariant mass. The reduced efficiency of the tight with respect to the standard SVX selection is understood in terms of dead regions in the first two silicon layers and is accurately modeled by the detector simulation on a run-by-run basis.

ment selects muon parent particles which decayed within a distance of $\simeq$ 1.5 cm from the nominal beam line, or in other words inside the beam pipe. According to the simulation, approximately 96% of dimuons due to known P+HF processes satisfy this condition. The standard SVX selection accepts muons from parent particles with a decay length as long as $\simeq$ 10 cm. The CDF measurements in Refs. [4,7] use slightly different tracking detectors, but their track selection criteria yield a decay-length acceptance quite similar to that of the standard SVX selection in the present study. The D0 study in Ref. [8] accepts muons from any decay length.

The acceptance of the different SVX selections as a function of the decay length of the muon parent particle is illustrated by using cosmic muons that overlap in time with a $p\bar{p}$ collision (for this purpose we remove the request that the azimuthal angle between two primary muons be less than 3.135 radians). Cosmic muons, which are reconstructed as two back-to-back muons of opposite charge, cluster along the diagonal of the two-dimensional distribution of the muon impact parameters. As shown in Fig. 2, the standard SVX selection accepts larger decay lengths than the tight SVX selection. As shown by the scatter of the points along the $d_1 = d_2$ diagonal, both SVX selections yield comparable rms resolutions that are negligible on a scale of the order of centimeters.

The efficiency of the tight SVX requirements for prompt dimuons is purely geometrical, and is measured to be 0.257 ± 0.004 by using $\Upsilon(1S)$ candidates [6]. For dimuons arising from heavy flavor production, the efficiency of the tight SVX selection is determined to be 0.237 ± 0.001 by using muons from J/ψ decays after reweighting their p_T distribution to be equal to that of muons from simulated decays of heavy flavors [4]. As shown by Fig. 3 (a), the 7% decrease of the efficiency for heavy flavors is due to a small fraction of high-p_T b hadrons decaying after the first SVXII layer. Using the sample composition determined by the fit to the muon impact parameter distribution, listed in Table 1, we estimate that $(24.4 \pm 0.2)\%$ of the initial P+HF contribution should survive the tight SVX requirements. The efficiency of the standard SVX selection is much higher and does not depend on the dimuon invariant mass. By using $\Upsilon(1S)$ and J/ψ candidates, we measure the efficiency of the standard SVX requirements to be 0.88 ± 0.01.

If the dimuon sample before the tight SVX selection (743006 events) had the same composition of the sample listed in Table 1 (143743 events), the average efficiency of the tight SVX requirements in this data set would be 0.244 ± 0.002, whereas it is found to be 0.1930 ± 0.0004. This feature suggests the presence of a large background which, unlike the P+HF contribution, is significantly sup-

[4] This efficiency has been independently verified using identified $B^{\pm} \to \mu^+\mu^- K^{\pm}$ and $B \to \mu D^0$ decays.

pressed by the tight SVX selection because most primary muons originate beyond the beam pipe. Because it went unnoticed for a long time, this background will be whimsically referred to as the ghost contribution in the following. In the assumption that the contribution of ghost events to the dimuon sample selected with tight SVX requirements is negligible, the size of the ghost sample can be estimated as the difference between the number of muon pairs prior to any SVX requirements and the number of muons passing the tight SVX selection divided by the efficiency of the tight SVX requirement. In order to compare with the result of previous measurements, we also extrapolate the contribution of ghost events to events in which the trigger muons pass the standard SVX selection. In this case, the ghost contribution is the difference between the numbers of events that pass the standard SVX requirements and that pass the tight SVX requirements scaled by the ratio of the efficiencies of the standard to tight SVX requirements. Throughout this article, the expected P+HF contribution and its characteristics will be always estimated from the sample of dimuons surviving the tight SVX requirements and properly accounting for the relevant SVX efficiencies averaged over the sample composition derived from the fits of Ref. [6]. The size of the ghost contribution and its kinematic properties will always be estimated by subtracting the expected P+HF contribution from the data sample prior to any SVX selection. Since the sample in which both trigger muons pass the tight SVX requirement is well modeled by the various P+HF contributions [6], it seems reasonable to start with the assumption that the ghost contribution in that sample is negligible. This procedure also allows an estimate of the number and properties of ghost events solely based on the data.

Table 2 lists the number of ghost events that pass different SVX requirements. In Table 2, the size of the ghost sample (153895 ± 4829 events) is of a magnitude comparable to $b\bar{b}$ production (221564 ± 11615 events). When using the standard SVX requirements, the size of the ghost sample is reduced by a factor of two, whereas 88% of the dimuons due to known processes survive (the ghost size is 72553 ± 7264 events, whereas the $b\bar{b}$ contribution is 194976 ± 10221 events). In order to later discuss the effect of ghost events on the $\bar{\chi}$ measurements at hadron colliders, we also provide event yields separately for the subset of events in which the dimuons have opposite-sign (OS) and same-sign (SS) charge. The ratio of OS to SS dimuons is approximately 2:1 for P+HF processes and 1:1 for ghost events.

Since this type of event has not been noticed by previous experiments, we have investigated at length the possibility that ghost muons are a consequence of the experimental conditions of the present study. The appearance of ghost events does not depend on the instantaneous luminosity nor the presence of multiple $p\bar{p}$ interactions. We have investigated in many ways the possibility that ghost events are ordinary P+HF events in which one of the primary muons appears to originate beyond the beam-pipe radius because of pattern recognition problems in the SVX or COT detectors (see Appendix A). It is our conclusion that ghost events are not due to track reconstruction failures in normal P+HF events. As an example, we select $B \to \mu D^0 X$ candidate decays and compare yields of $D^0 \to K^-\pi^+$ (and charge-conjugate) decays in P+HF and ghost events. We search for D^0 candidates by using tracks of opposite sign charge, with $p_T \geq 1.0$ GeV/c, $|\eta| \leq 1.1$, and contained in a 60° cone around the direction of each primary muon. The two-track systems are constrained to arise from a common space point. Track combinations are discarded if the three-dimensional vertex fit returns a χ^2 larger than 10 or if the vertex is not in the hemisphere containing the D^0 candidate. We attribute the kaon mass to the track with the same charge as the primary muon (RS combination, as expected for $B \to \mu^- D^0$ decays). We also study wrong sign combinations (WS) attributing the kaon mass to the track with opposite charge. A D^0 signal in WS combinations in P+HF events is a measure of the fake muon contribution, whereas a D^0 signal in ghost events would be an indication of misrecontructed muon tracks in events with heavy flavors. As shown in Figs. 4 (a) and (b), a clear D^0 signal is only observed in RS combinations in P+HF events.

Table 2. Number of events that pass different SVX requirements. P+HF indicates the sum of the various components listed in Table 1. Ghost indicates the contribution ignored by previous experiments. Dimuons are also split into pairs with opposite (OS) and same (SS) sign charge.

Type	Total	Tight SVX	Standard SVX
All	743006	143743	590970
All OS		98218	392020
All SS		45525	198950
P+HF	589111 ± 4829	143743	518417 ± 7264
P+HF OS		98218	354228 ± 4963
P+HF SS		45525	164188 ± 2301
Ghost	153895 ± 4829	0	72553 ± 7264
Ghost OS		0	37792 ± 4963
Ghost SS		0	34762 ± 2301

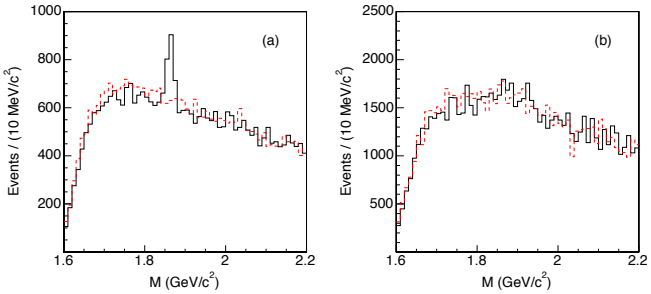

Fig. 4. Invariant mass, M, distributions of RS (histogram) and WS (dashed histogram) D^0 candidates in (a) P+HF and (b) ghost events.

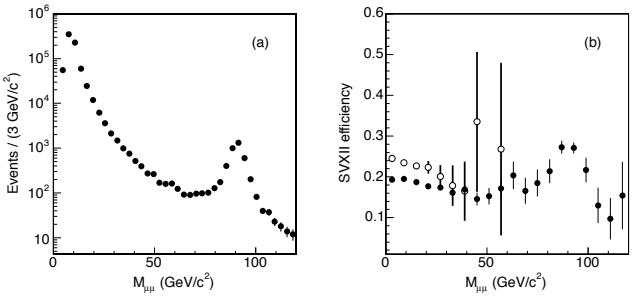

Fig. 5. Invariant mass distribution (a) of the dimuon pairs used in the study. The efficiency (b) of the tight SVX requirements as a function of the dimuon invariant mass in the data (•) is compared to that in the heavy flavor simulation (○).

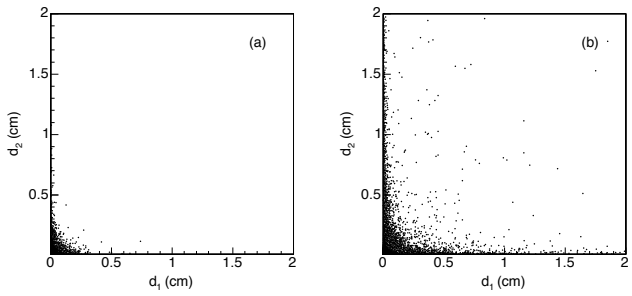

Fig. 6. Two-dimensional impact parameter distribution of dimuons that pass the (a) tight and (b) standard SVX requirements.

4.1 Ordinary sources of ghost events

In the following, we investigate several sources of ghost events that might not have been properly accounted for by previous experiments: (a) semileptonic decays of hadrons with an unexpectedly large Lorentz boost; (b) muonic decays of particles with a lifetime longer than that of heavy flavors, such as K and π mesons; (c) decays of K^0_S mesons and hyperons; and (d) secondary interactions of hadrons that occur in the detector volume. In the last two cases, muons are predominantly produced by punchthrough of the secondary prongs that penetrate the calorimeter and hit the muon detectors.

Figure 5 shows the invariant mass of dimuon pairs before the tight SVX selection, and the efficiency of this selection as a function of the dimuon invariant mass. The efficiency of the tight SVX requirements in the data is below that in the simulation only for dimuon invariant masses smaller than 40 GeV/c^2, and then rises to the expected value of 0.257 where events are mostly contributed by prompt Z^0 decays. This feature does not favor hypothesis (a).

A long-lived particle contribution is suggested by the comparison of the impact parameter distribution of dimuons that pass the standard and tight SVX requirements in Fig. 6. Figure 7 shows impact parameter distributions of trigger muons selected with standard SVX requirements in P+HF and ghost events. The two distributions are completely different, and the average impact parameter of ghost muons is significantly larger than that of muons due to P+HF production. Previous experiments [4,7] have determined the dimuon sample composition by fitting the distribution of muon impact parameters smaller than 0.2 cm with templates for muons due to prompt, c- and b-quark production. Therefore, these fits attribute the ghost component to b-quark production, the source with the longest lifetime; and the resulting $b\bar{b}$ cross section is augmented by the ratio of ghost to $b\bar{b}$ events in that sample which in turn depends on the SVX requirements applied to the trigger muons.

According to the heavy flavor simulation [6], dimuons with impact parameter larger than 0.12 cm only arise from $b\bar{b}$ production. We fit the impact parameter distribution

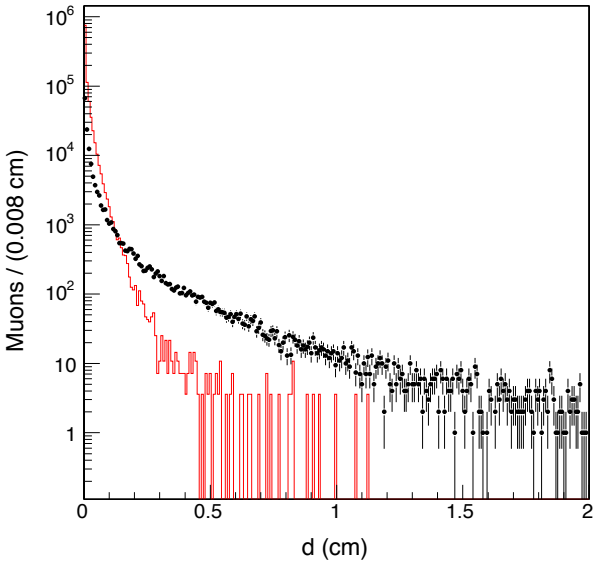

Fig. 7. Impact parameter distribution of muons contributed by ghost (•) and P+HF (histogram) events. Muon tracks are selected with standard SVX requirements. The detector resolution is $\simeq 30$ μm, whereas bins are 80 μm wide.

in Fig. 8 with the function $A\exp(-d/(c\tau))$ in the range $0.12-0.4$ cm. The best fit returns $c\tau = 469.7 \pm 1.3$ μm in agreement with the value 470.1 ± 2.7 μm expected for the b-hadron mixture at the Tevatron [5]. We conclude that the data sample selected with the tight SVX selection is not appreciably contaminated by ghost events. This supports our initial assumption that the ghost contribution to events selected with tight SVX requirements is negligible. It also follows that the $b\bar{b}$ contribution to dimuons with impact parameter larger than 0.5 cm is negligible.

In ghost events, the presence of a significant tail extending to large impact parameters suggests the contribution of particles with a lifetime much longer than that of b quarks, such as K^0_S, K and π mesons, and hyperons. We first investigate muons produced by pion and kaon in-flight-decays [source (b)]. As reported in Ref. [6], af-

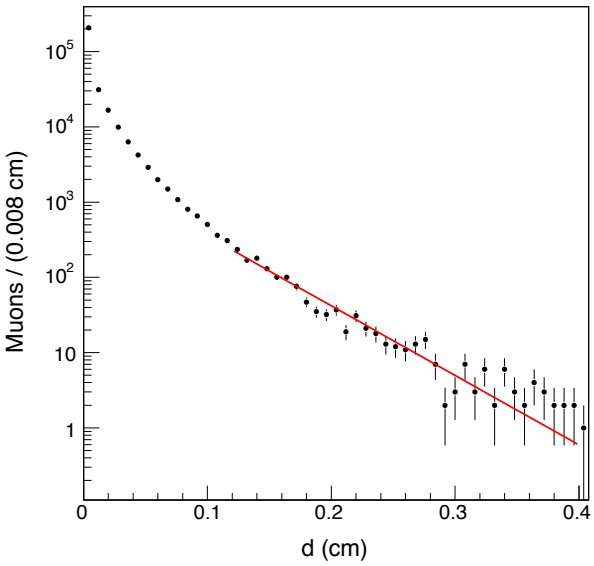

Fig. 8. Impact parameter distribution of muons that pass the tight SVX requirements. The line represents the fit described in the text.

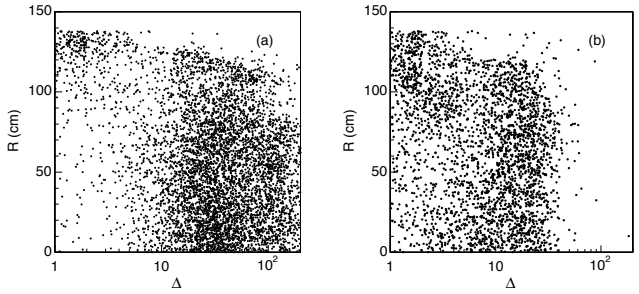

Fig. 9. Distribution of Δ (see text) as a function of the distance R of the (a) K and (b) π decay vertices from the nominal beamline. For comparison, the analogous distribution for real muons from heavy flavor decays does not extend beyond $\Delta = 9$.

Table 3. Number of pions and kaons corresponding to a misreconstructed track ($\Delta \geq 5$) with $p_T \geq 3$ GeV/c and $|\eta| \leq 0.7$, that decay inside the tracking volume, produce CMUP muons with a L1 primitive, and pass different SVX selections.

Selection	π	K
Tracks	2667199	1574610
In-flight-decays	14677	40561
CMUP+L1	1940	5430
Standard SVX	897	3032
Tight SVX	319	1135

ter having selected muon pairs with the tight SVX requirements, approximately 30% of the P+HF contribution is due to prompt hadrons mimicking a muon signal. The size of the ghost sample has been estimated assuming that the efficiency of the tight SVX requirements for these tracks is the same as that for real muons. This is a reasonable assertion when fake muons are generated by hadronic punchthroughs. However, muons arising from π or K decays inside the tracking volume may yield misreconstructed tracks that are linked to hits in the SVXII detector less efficiently than real muons. We estimate this efficiency using pions and kaons produced in the large statistics heavy flavor simulation used to derive the dimuon acceptance for the $\sigma_{b\to\mu,\bar{b}\to\mu}$ measurement [6]. We use the quantity $\Delta^2 = 1/3 \cdot [(\eta^h - \eta^{\rm track})^2/\sigma_\eta^2 + (\phi^h - \phi^{\rm track})^2/\sigma_\phi^2 + (1/p_T^h - 1/p_T^{\rm track})^2/\sigma^2_{1/p_T}]$ to measure the difference between the momentum vectors of the undecayed pions or kaons (h) and that of the closest reconstructed tracks [5]. Figure 9 shows the Δ distribution as a function of R, the decay distance from the detector origin (nominal beamline) in the transverse plane. Contradicting the assumption of previous experiments, most of the decays at radial distances $R \leq 120$ cm are reconstructed as single tracks that unfortunately differ significantly from that of the undecayed pions or kaons which left hits in the silicon detector. The numbers of in-flight-decays that produce CMUP muons with $p_T \geq 3$ GeV/c, a L1 primitive, and which pass different SVX selections are listed in Table 3. The efficiency of the tight SVX requirements for a single muon due to in-flight-decays (0.16 and 0.21 for π and K decays, respectively) is smaller than that for muons in P+HF events ($\simeq 0.5$).

The contribution of in-flight-decays to ghost events is evaluated using simulated events produced in generic-parton scattering [6]. In the generic-QCD simulation, there are 44000 track pairs per CMUP pair due to $b\bar{b}$ production with the same kinematic acceptance ($p_T \geq 3$ GeV/c and $|\eta| \leq 0.7$). The ratio of the number of pions to that of kaons is approximately 5:1. Each simulated track in the kinematic acceptance is weighted with the corresponding in-flight-decay probabilities of producing CMUP muons listed in Table 3. Tracks are also weighted with the probabilities, measured in Ref. [6], that π or K punchthrough mimics a CMUP signal. In the latter case, the efficiency of the SVX requirement is the same as for real muons, and we ignore the cases in which both muons arise from hadronic punchthrough. Having normalized this simulation to the number of observed primary muons arising from $b\bar{b}$ production, we predict a contribution to ghost events due to in-flight-decays of pions and kaons that is 57000 events, 44% and 8% of which pass the standard and tight SVX selection, respectively. In the 25000 simulated events that pass the standard SVX selection, approximately 15000 muons arise from kaon in-flight-decays. This prediction depends on how well the HERWIG generator models kaon and pion production in final states due to

[5] The assumed experimental resolutions are $\sigma_\phi[\text{rad}] = \sigma_\eta = 10^{-3}$ and $\sigma_{1/p_T} = 2 \cdot 10^{-3}$ [GeV/c]$^{-1}$.

[6] We use option 1500 of the HERWIG program to generate final states produced by hard scattering of partons with transverse momentum larger than 3 GeV/c [6].

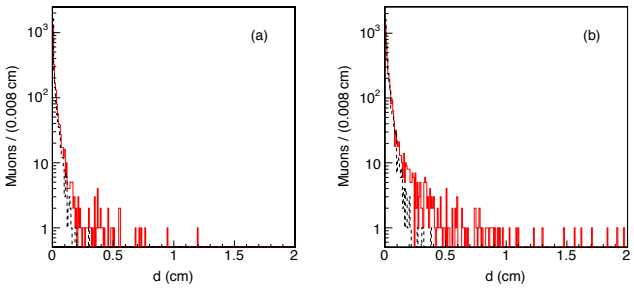

Fig. 10. Impact parameter distributions of simulated CMUP muons (histogram) that pass all analysis requirements, including the standard SVX selection, and arise from (a) pions and (b) kaon in-flight decays. The dashed histograms show the impact parameter of the parent pions and kaons.

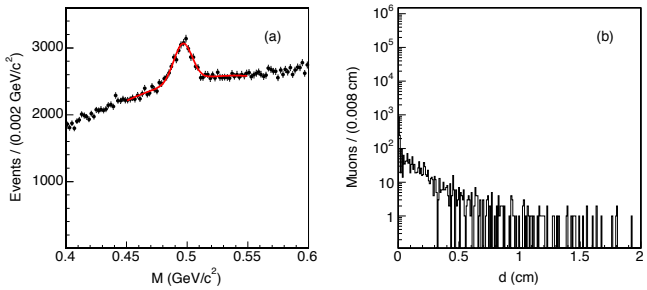

Fig. 11. Distributions of (a) the invariant mass of pairs of primary muons and opposite sign tracks and of (b) the impact parameter of primary muons, produced by K^0_S decays, that pass the standard SVX selection. The solid line represents a fit described in the text. In the impact parameter distribution, the combinatorial background is removed with a sideband subtraction method. For comparison, the vertical scale in (b) is kept the same as in Fig. 7.

low-p_T generic-parton scattering and its uncertainty is difficult, when not impossible, to estimate. Figure 10 shows the impact parameter distribution of muons arising from in-flight-decays of pions and kaons produced in simulated $b\bar{b}$ and $c\bar{c}$ events. The number of events in Fig. 10 has to be multiplied by five in order to be compared with the data in Fig. 7. Our estimate of the number of muons arising from in-flight-decays accounts for 35% of the ghost muons, but for less than 10% of those with $d \geq 0.5$ cm.

In addition, muons in ghost events can be mimicked by the punchthrough of hadrons arising from the decay of K^0_S mesons or hyperons [source (c)]. We have searched the dimuon data set for $K^0_S \rightarrow \pi^+\pi^-$ decays in which a pion punchthrough mimics the muon signal. We combine all primary muon tracks with all opposite sign tracks with $p_T \geq 0.5$ GeV/c contained in a 40° cone around the direction of the primary muons. Muon-track combinations are constrained to arise from a common space point. They are discarded if the three-dimensional vertex fit returns a χ^2 larger than 10. Figure 11 (a) shows the invariant mass distribution of the K^0_S candidates reconstructed assuming that both tracks are pions. A fit of the data with a Gaussian function to model the signal plus a second order polynomial to model the background yields a signal of 5348 ± 225 K^0_S mesons. The impact parameter distribution of primary muons produced by K^0_S decays is shown in Fig. 11 (b). The data also contain a smaller number of cases in which the primary muon is mimicked by the products of hyperon decays. Using a similar technique, we have searched the data for $\Lambda \rightarrow p\pi^-$ (and its charge-conjugate) decays and we find a signal of 678 ± 60 Λ baryons (see Fig. 12). Since in both cases the kinematic acceptance times reconstruction efficiency is approximately 50%, source (c) ($\simeq$ 12000 events) explains $\simeq$ 8% of the ghost events.

The final source (d) of ghost events, secondary interactions in the detector volume, is investigated using the data. We search for secondary interactions by combining primary muons with any track with $p_T \geq 0.5$ GeV/c contained in a 40° cone around the muon direction. We retain combinations that are consistent with arising from a common space point. The distribution of R, the distance of a reconstructed secondary vertex from the nominal beamline, is shown in Fig. 13. The distance R is negative when the secondary vertex is in the hemisphere opposite to that containing the momentum of the muon-track system. Secondary inelastic interactions are characterized by narrow spikes at R values where the detector material is concentrated, such as SVX supports or the COT inner support cylinder, and are appreciable in both data and simulated events when secondary vertices are reconstructed using pairs of hadronic tracks rather than muon-track pairs (see

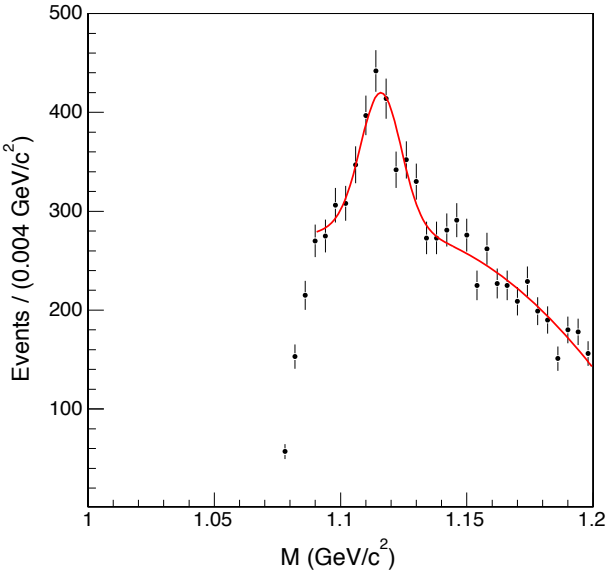

Fig. 12. Distributions of the invariant mass of pairs of primary muons and opposite sign tracks regarded as proton-pion and pion-proton pairs. The solid line represents a fit that uses a Gaussian function to model the Λ signal and a fourth order polynomial to model the combinatorial background.

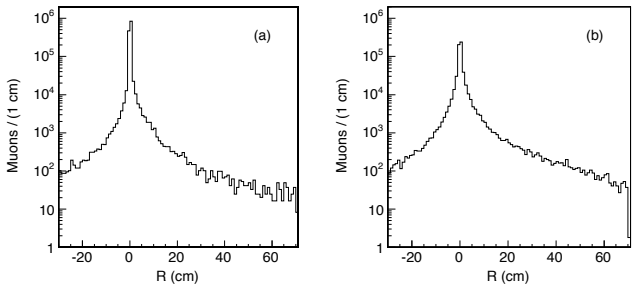

Fig. 13. Distributions of R, the signed distance of muon-track vertices from the nominal beamline for (a) P+HF and (b) ghost events (see text).

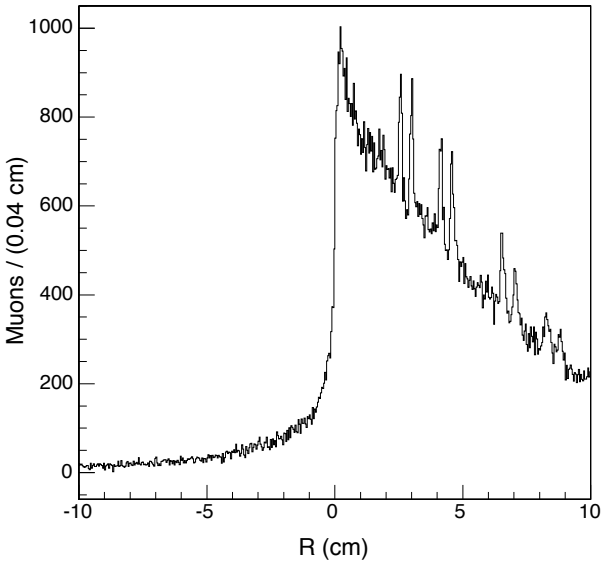

Fig. 14. Distributions of R, the signed distance of two-track vertices from the nominal beam line in simulated events in which hadron pairs are produced by the decay of an object with a 20 ps lifetime. Spikes correspond to the location of the different silicon layers and their mechanical supports. In the heavy flavor simulation, the efficiency for reconstructing inelastic interactions which produce at least a prong with $p_T \geq 3$ GeV/c is approximately 80%.

Fig. 14). From the absence of visible spikes, we conclude that the contribution of secondary inelastic interactions is negligible. This does not exclude contributions from elastic or quasi-elastic nuclear scattering of hadronic tracks in the detector material. However, in the momentum range of tracks and muons considered in this study, the elastic and quasi-elastic production are known to be small compared to the inelastic cross section [28].

Our estimate underpredicts the observed number of ghost events by approximately a factor of two (154000 observed and 69000 accounted for). However, given the possible large uncertainty of the in-flight-decay prediction, at this point of our study we cannot exclude that the size of ghost sample can be completely accounted for by a combination of all the above-studied background sources. In other word, the systematic uncertainty of our prediction could be as large as the difference between the data and the prediction.

Although we cannot model the size of the ghost sample in terms of known sources, the identification of this type of event provides a plausible resolution to most of the inconsistencies mentioned in the introduction. The general observation is that the measured $\sigma_{b\to\mu,\bar{b}\to\mu}$ increases as the trigger muons are allowed to originate at increasing distances from the primary event vertex, and is almost a factor of two larger than that measured in [6] when no distance requirement is made [8]. As mentioned above, the magnitude of the ghost contribution is comparable to the $b\bar{b}$ contribution when no SVX selection is made and in combination would account for the measurement reported in [8]. Similarly, for the standard SVX criteria, the magnitude of the ghost contribution (72553 ± 7264 events, equally split in OS and SS dimuons), when added to the $b\bar{b}$ contribution of 194976 ± 10221 events [6], coincides with the cross section measurement reported in [7] and the $\bar{\chi}$ value reported in [4] since these measurements use similar sets of SVX requirements.

Ghost events due to these ordinary sources are not expected to contain a number of additional muons comparable to that of events due to $b\bar{b}$ production. Therefore, these sources cannot be the origin of the excess of low-mass dileptons reported in Ref. [3]. That study is repeated in the next section to verify the discrepancy itself and then a possible connection to the presence of ghost events.

5 Study of events that contain an additional muon

We begin this study with events that contain a pair of primary muons passing our analysis selection without any SVX requirements. We then search for additional tracks with $p_T \geq 2$ GeV/c and a matching stub in the CMU, CMX, or CMP muon detectors (the three detectors cover the pseudorapidity region $|\eta| \leq 1.1$). No SVX requirements are made on these additional muons. This type of muon selection provides a detector and kinematic acceptance five times larger than that for trigger muons at the price of a tenfold increase of the probability that hadronic tracks penetrate the calorimeter and mimick a muon signal. Since additional muons are searched for offline and there are no trigger rate limitations, this method is the one customarily used by CDF analyses to tag semileptonic decays of heavy flavors [3,4,25]. For muons with $p_T \geq 2$ GeV/c and $|\eta| \leq 1.1$, the muon detector efficiency in the heavy flavor simulation is 0.805 ± 0.008. We measure the muon detector efficiency in the data by using J/ψ candidates acquired with the μ-SVT trigger (see Ref. [6] for more details). After reweighting the kinematics of the muons from J/ψ decays to reproduce that of simulated muons from heavy flavor decays, the efficiency is measured to be 0.838 ± 0.004.

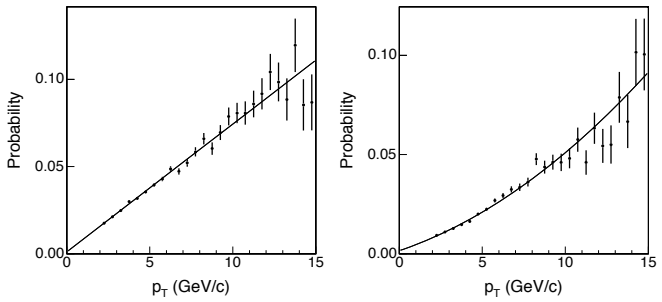

Fig. 15. Probability that a track with $|\eta| \leq 1.1$ penetrate the calorimater and mimics a muon signal in the CMU, CMX, or CMP detectors as a function of the kaon (left) or pion (right) transverse momentum. As expected for fakes due to hadronic punchthrough, the fake probabilities do not depend on the SVX requirements applied to the tracks.

According to the heavy flavor simulation, additional real muons predominantly arise from sequential decays of single b hadrons (the $g \to b\bar{b}$ and $g \to c\bar{c}$ contributions are suppressed by the request of two primary muons with $p_T \geq 3$ GeV/c, $|\eta| \leq 0.7$, and invariant mass larger than 5 GeV/c^2). In addition, one expects a contribution of fake muons from hadrons mimicking the muon signal. The CDF II detector simulation does not describe hadronic punchthrough. As customarily done in CDF analyses that identify b quarks through their semileptonic decays, the fake muon contribution is evaluated by weighting each pion and kaon candidate track in the simulation with the probability of penetrating the calorimeter and mimicking a muon signal. These fake probabilities, shown in Fig. 15 as a function of the track p_T, have been measured using a sample of $D^0 \to K^-\pi^+$ decays acquired with the CHARM and μ-SVT triggers. The procedure for determining these probabilities is described in detail in Appendix B of Ref. [6].

Requesting the presence of at least one muon in addition to the two primary muons modifies the sample composition relative to the initial sample and is expected to enhance the $b\bar{b}$ contribution. After correcting for fake muons, we expect $b\bar{b}$ production to dominate the sample with three or more muons. In events containing an $\Upsilon(1S)$ candidate, that are included in the dimuon sample, the probability of finding an additional muon is $(0.90 \pm 0.01)\%$. Of the 5348 ± 225 events with an identified K^0_S meson only 94 ± 41, or $(1.7 \pm 0.8)\%$, survive the request of an additional muon in the event.

In the data, 9.7% of the dimuon events contain an additional muon (71835 out of 743006 events). When comparing the efficiencies of the tight SVX requirements applied to primary muon pairs, we observe the efficiency to drop from $(19.30 \pm 0.04)\%$ in the full sample to $(16.6 \pm 0.1)\%$ in the subsample that contains at least one additional muon. The drop of the SVX efficiency is a direct indication that ghost events are a larger fraction of the sample containing additional muons. The ghost contribution accounts for $(20.9 \pm 0.8)\%$ of the dimuon sample prior to any SVX requirements. When we request the presence of additional muons, the ghost contribution accounts for $(32.0 \pm 0.7)\%$ of the surviving sample. In other words, ghost events contain more additional muons than the P+HF contribution.

Following the study in Ref. [3], additional muons are paired with one of the primary muons if their invariant mass is smaller than 5 GeV/c^2. For this study, we use a larger statistics data sample [7]. Following the analysis procedure of Ref. [3], we retain muon combinations with charges of opposite sign (OS). As in Ref. [3], we estimate the contribution of fake muons from the number of same sign (SS) muon pairs. In the case of Drell-Yan or quarkonia production, fake additional muons arise from the underlying event and one expects no charge correlation between primary and additional fake muons. In the simulation of heavy flavor decays, most tracks surrounding a muon arise from the fragmentation and decay of the same b or c-quarks that produced the primary muons. In this case, the ratio of OS to SS muon-track combinations as well as the ratio of the numbers of pion to kaon tracks is a function of the invariant mass of the muon-track pair. Since pions and kaons have different fake probabilities, the number of OS and SS pairs due to fake muons needs to be also evaluated in simulated events due to heavy-flavor production.

The rate of real plus fake muon pairs with small invariant mass is evaluated after rescaling the parton level cross section predicted by the HERWIG generator to match the measurements $\sigma_{b\to\mu,\bar{b}\to\mu} = 1549 \pm 133$ pb and $\sigma_{c\to\mu,\bar{c}\to\mu} = 624 \pm 104$ pb [6]. In the simulation, the pair of primary muons is always arising from heavy-flavor semileptonic decays. In the data, 9% of the primary muons recoiling against a small mass dimuon are due to prompt hadrons mimicking the muon signal (relative size of the BB and BP components in Table 1). In addition, 2% of these recoiling muons are due to hadrons from heavy flavor decays [6]. We account for this by increasing the rates predicted by the simulation by a factor of 1.12.

As in the data, SS combinations due to either real or fake muon pairs are subtracted from OS combinations. Figure 16 shows the ratio of the total number of $OS - SS$ muon pairs predicted by the above calculation to that of real $OS - SS$ dimuons from heavy flavor decays. The integrated fake contribution is approximately 33% of that of real muons from sequential decays of single b quarks. Figure 17 compares the invariant mass spectrum of $OS - SS$ muon pairs in the data and in the heavy flavor simulation. Since the simulation is effectively normalized to the observed number of primary muon pairs, the prediction has a 3% systematic error due to the branching ratio $b \to c \to \mu$ plus a 3% uncertainty due to the absolute pion and kaon rates predicted by the simulation [6] (the systematic uncertainty of the muon detector efficiency is

[7] The correlated $b\bar{b}$ cross section measurement uses 742 pb^{-1} of data in which the dimuon trigger is not prescaled as a function of the instantaneous luminosity. From the total number of dimuon events that pass the same analysis selection, the luminosity of this larger data sample is estimated to be 1426 pb^{-1}.

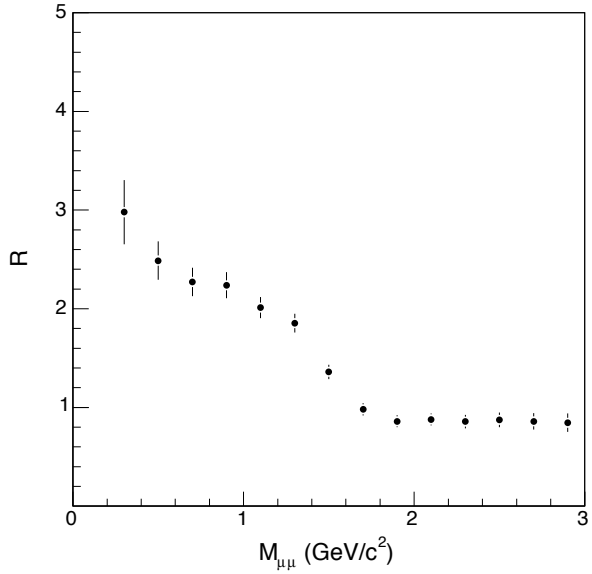

Fig. 16. Ratio (R) of total number of $OS-SS$ muon pairs to that of real $OS-SS$ pairs arising from heavy flavor decays as a function of the dimuon invariant mass. We use simulated events generated with the HERWIG Monte Carlo program. The generator parton-level cross sections have been scaled to match the data [6]. The number of fake muon pairs has been evaluated by weighting simulated hadronic tracks with the probability of mimicking a muon signal as measured with data.

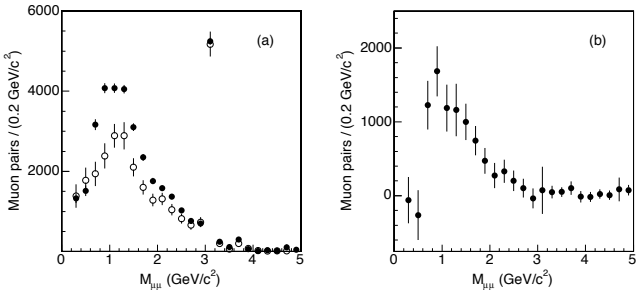

Fig. 17. The invariant mass distribution of (a) $OS-SS$ muon pairs in the data (•) is compared to the simulation prediction (○). One of the two primary muons in the event is combined with an additional muon if their invariant mass is smaller than 5 GeV/c^2. The difference (b) between data and prediction is also shown.

negligible). This systematic uncertainty is not shown in Fig. 17. The number of J/ψ mesons in the data is correctly modeled by the simulation in which J/ψ mesons only arise from $b\bar{b}$ production. The agreement between the number of observed and predicted J/ψ mesons selected without any SVX requirement supports the estimate of the efficiency of the tight SVX requirement and the resulting value of the correlated $b\bar{b}$ cross section reported in Ref. [6]. However, the data are underestimated by the simulation for invariant masses smaller than 2 GeV/c^2. The

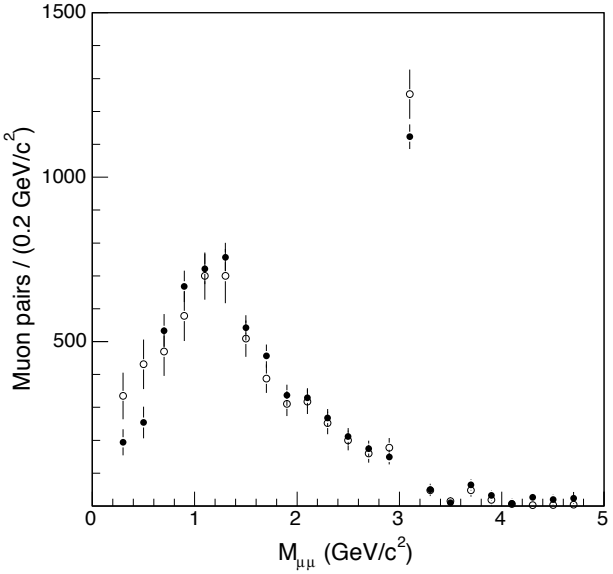

Fig. 18. The invariant mass distribution of $OS-SS$ muon pairs in the data (•) is compared to the simulation prediction (○). Primary muons are selected using the tight SVX requirements.

excess of 8451 ± 1274 events results from an observation of 37042 ± 389 and a prediction of 28589 ± 1213 events. The size and shape of the excess is consistent with what was first reported in Ref. [3], in which the excess was mostly observed in a high statistics $e\mu$ sample.

This excess is produced by ghost events. When the primary muons are selected with the tight SVX requirements, we observe 6935 ± 154 events, whereas 6918 ± 293 are predicted. The corresponding invariant mass distribution is shown in Fig. 18. The rate of $OS-SS$ pairs per event in the ghost sample (8451 ± 1274 pairs in 295481 ± 9271 events) is larger than that in P+HF events (6935 ± 154 in 275986 events). Thus far, we have established that ghost events contain more additional muons than $P+HF$ sources. The ghost sample is now understood to be the source of the dimuon invariant mass discrepancy reported in Ref. [3] even if a large but uncertain fraction of ghost events is due to in-flight-decays which cannot account for a rate of additional muons higher than that of $b\bar{b}$ production. In the following sections, we further investigate the properties of this subset of ghost events.

5.1 Kinematics of additional muons in ghost events

The excess of 8451 ± 1274 $OS-SS$ pairs with invariant mass smaller than 5 GeV/c^2 in 295481 ± 9271 ghost events is slightly higher than that observed in events in which primary muons survive the tight SVX selection (6935 ± 154 $OS-SS$ pairs in 275896 events). For the latter events, SS pairs are accounted for by the fake probability per track applied to the data and the heavy flavor simulation. Since

Table 4. Number of events as a function of N_c, the number of combinations of primary and additional muons. Additional muons are combined with primary muons if the pair invariant mass is smaller than 5 GeV/c^2. The number of combinations are also split into opposite (OS) or same (SS) sign charge. "SVX" are numbers of events that pass the tight SVX selection. P+HF is the latter number divided by the efficiency of the tight SVX requirements. Ghost is the difference between the total and the P+HF contributions.

Topology	Total	SVX	P+HF	Ghost
$N_c \geq 0$	1426571	275986	1131090 ± 9271	295481 ± 9271
$N_c \geq 1$	141039	22981	94184 ± 772	46855 ± 772
OS	94148	15372	63000 ± 516	31148 ± 516
SS	57106	8437	34578 ± 283	22528 ± 283
$N_c \geq 2$	10215	828	3393 ± 28	6822 ± 28

we do not know the composition of the ghost sample and are incapable of modeling it with a simulation, the excess of $OS-SS$ pairs in Fig. 17 represents nothing more than a measure of the charge asymmetry of additional muons as a function of the invariant mass of the muon pair. However, we can estimate the fake rate in ghost events from the data under different assumptions.

In 1,426,571 dimuon events, we find 94148 OS and 57106 SS combinations with an additional muon with $m_{\mu\mu} \leq 5$ GeV/c^2. A qualitative estimate predicts that 14200 SS and OS fake muon combinations are produced by the underlying event [8]. The heavy flavor simulation, which also accounts for fake muons, predicts 40899 OS and 12309 SS real plus fake combinations for a grand total of 55100 OS and 26500 SS pairs. This approximate prediction underestimates the data by 39000 OS and 30500 SS pairs.

The number of the OS and SS pairs in ghost events is determined more precisely as the difference between the data and the P+HF expectation. This study is summarized in Table 4. In ghost events, the fraction of events that carries an additional real or fake muon with any charge is $(15.8 \pm 0.3)\%$, approximately a factor of two higher than in P+HF events. Before estimating the fraction of additional muons due to tracks mimicking a muon signal, we need to investigate one of the kinematic requirements thus far used to select dimuon pairs.

In order to compare with the previous measurement [3], we have selected dimuon pairs with $m_{\mu^+\mu^-} \leq 5$ GeV/c^2. This requirement is survived by dimuons produced by sequential semileptonic decays of single b-quarks, but could bias the investigation of ghost events. Therefore, we search dimuon events for additional muons without any invariant mass cut. If the primary dimuon pair has opposite charge, we combine the additional muon with the primary muon of opposite charge (OSO combinations). If the primary muons have same charge, we randomly combine the additional muon with one of the primary muons (SSO and SSS combinations). The number of three-muon combinations is listed in Table 5 [9]. Figure 19 shows the invariant mass and opening angle distribution of OSO combinations for the P+HF and ghost contributions. Muon pairs due to b sequential decays, which account for most of the P+HF contribution, peak at small invariant masses and small opening angles. The tail at large masses and opening angles results from fake muons with wrong charge. The distributions of analogous pairs in the ghost sample have

Table 5. Numbers and types of three-muon combinations. We separate events according to the charge of the primary muons. The topology OSO is that of two opposite-charge primary dimuons; by definition, the third muon has opposite charge with respect to one of them. When primary dimuons have same sign charge, the third muon charge can have either the same (SSS) or opposite sign (SSO).

Topology	All	SVX	P+HF	Ghost
OSO	90022	14497	59414 ± 487	30608 ± 487
SSO	48220	7708	31590 ± 259	16630 ± 259
SSS	28239	4139	16963 ± 139	11276 ± 139

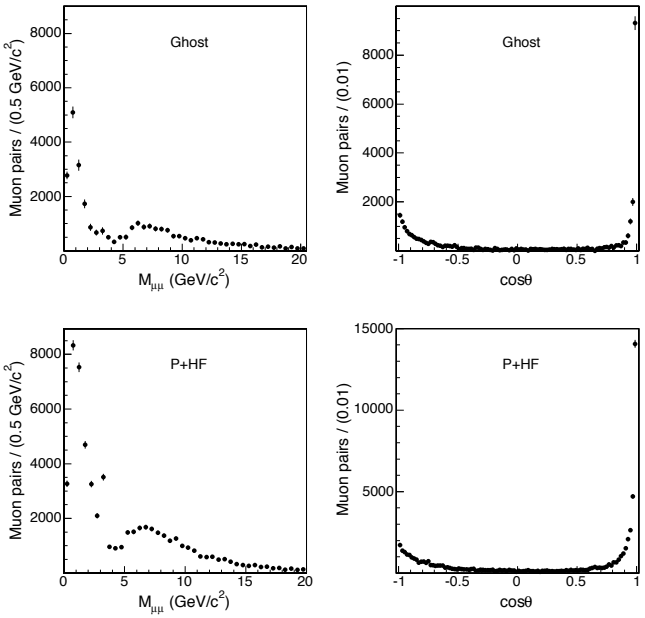

Fig. 19. Events with OS primary muon pairs and an additional muon combined with the opposite-charge primary muon. We show the invariant mass, $M_{\mu\mu}$, and opening angle, θ, distributions of these combinations for the P+HF and ghost contributions.

[8] These numbers are derived from the 1% probability of finding an additional muons in events with $\Upsilon(1S)$ candidates and assuming that the underlying event is the same for all processes.

[9] The P+HF contribution is estimated as the number of combinations in events in which primary dimuons pass the tight SVX requirements (SVX) divided by the efficiency of the tight SVX requirements. As always, the ghost contribution is the difference between the data and the P+HF contribution.

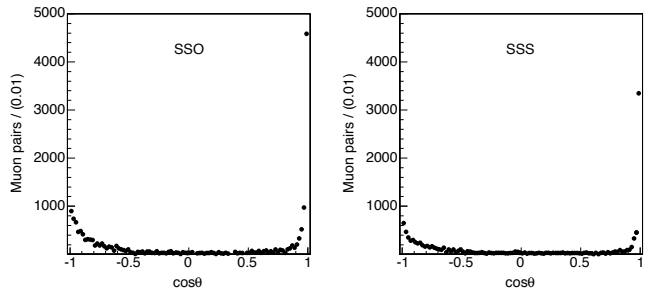

Fig. 20. Opening angle distributions of dimuon combinations for ghost events. The primary dimuons have same sign charge, and combinations of an additional and primary muons are split according to the charge of the additional muon. The plots are the projection of two-dimensional distributions in which the additional muon is combined with both primary muons.

Table 6. Numbers of additional muons with an angle $\theta \leq 36.8^{\circ}$ with respect to the direction of one of the primary muons. We list separately the combinations of additional and primary muons with opposite (OS) and same (SS) sign charge.

Topology	All	SVX	P+HF	Ghost
OS	83237	13309	54545 ± 447	28692 ± 447
SS	50233	7333	30053 ± 246	20180 ± 246

a quite similar behaviour. However, combinations of primary and additional muons in ghost events have a smaller opening angle than those from sequential b decays. As shown in Fig. 20, SSO and SSS combinations have similar opening angle distributions. Therefore, it seems reasonable to restrict the study of ghost events to muons and tracks contained in a cone of angle $\theta \leq 36.8^{\circ}$, corresponding to $\cos\theta \geq 0.8$, around the direction of each primary muon.

6 Study of muon and track properties in ghost events

The number of additional muons contained in a cone of angle $\theta \leq 36.8^{\circ}$ ($\cos\theta \geq 0.8$) around the direction of any primary muon is listed in Table 6.

The contribution of fake muons is evaluated by weighting all tracks with $p_T \geq 2$ GeV/c, $|\eta| \leq 1.1$, and contained in a $\cos\theta \geq 0.8$ cone, with the fake probabilities shown in Fig. 15. Table 7 lists the number of these tracks for P+HF and ghost events. The P+HF and ghost contributions have been previously determined to be 1131090 and 295481 events, respectively. Therefore, the average number of tracks contained in a $\theta \leq 36.8^{\circ}$ cone around the direction of one of the primary muons in ghost events is 1.58 OS and 1.08 SS, twice the values measured in P+HF events (0.75 OS and 0.51 SS tracks).

For ghost events, Table 8 compares the observed number of additional muons to the number of fake muons predicted assuming that tracks are either all pions or all

Table 7. Numbers of tracks with $p_T \geq 2$ GeV/c, $|\eta| \leq 1.1$, and an angle $\theta \leq 36.8^{\circ}$ with respect to the direction of one of the primary muons. We list separately the numbers of tracks with opposite (OS) and same (SS) charge as the primary muon. Tracks associated with a muon stub are excluded.

Topology	All	SVX	P+HF	Ghost
OS	1315451	207344	849770 ± 6965	465860 ± 6965
SS	893750	140238	574745 ± 4711	318004 ± 4711

Table 8. Numbers of additional muons in ghost events are compared to fake muon expectations. The fake muon prediction is evaluated by applying the fake probabilities shown in Fig. 15 to all tracks not associated to a muon stub and with $p_T \geq 2$ GeV/c, $|\eta| \leq 1.1$, and an angle $\theta \leq 36.8^{\circ}$ with respect to the direction of one of the primary muons. We list separately the numbers of muons with opposite (OS) and same (SS) sign charge as the primary muon. F_K and F_π are the numbers of fake muons predicted assuming that hadronic tracks are all kaons or all pions, respectively. For kaon tracks, the rate of predicted fake muons should be increased by 10% to also account for in-flight-decay contributions.

Topology	Observed	F_K	F_π
OS	28692 ± 447	15447 ± 210	9649 ± 131
SS	20180 ± 246	10282 ± 137	6427 ± 81

kaons. The rate of additional real muons per ghost event, $(9.4 \pm 0.2)\%$, is obtained from the number of $OS + SS$ pairs minus the average of the pion and kaon fake contributions listed in Table 8. This rate is four times larger than that, $(2.16 \pm 0.05)\%$, of $OS - SS$ pairs in P+HF events in which SS pairs are properly accounted by the fake muon prediction (see Table 6). In Table 8, the ratio of real to fake muons in ghost event is approximately 1. The analogous ratio in P+HF events, which are correctly modeled by the heavy flavor simulation, is 0.4. Therefore, it seems difficult that the observation in ghost events may result from a systemic underprediction of the fake rate.

As a cross-check that the difference in rates of additional muons between the P+HF and ghost sample is contributed by real muons, we restrict our study to additional muons identified as CMUP muons. The numbers of additional CMUP muons and expected fakes are listed in Table 9. Using this muon selection, the fake contribution is much reduced at the expense of the muon acceptance that decreases by a factor of approximately five. The fraction of real additional CMUP muons is $(0.40 \pm 0.01)\%$ in P+HF events, and four times larger $(1.64 \pm 0.08)\%$ in ghost events. This result is consistent with the previous determination that uses all muon detectors.

Figure 21 (a) shows the distribution of the number of muons found in a $\cos\theta \geq 0.8$ cone around a primary muon due to ghost events. In the plot, an additional muon increases the multiplicity by 1 when of opposite sign and by

Table 9. Numbers of additional CMUP muons in P+HF and ghost events. F_π is the number of fake muons in ghost events, predicted assuming that hadronic tracks are pions. If tracks are assumed to be kaons, the fake probability per track is approximately four times higher after including the in-flight-decay contribution. In P+HF events, in which a large fraction of fake muons is due to kaons, the number of SS combinations underestimates the fake muon contribution to OS combinations by approximately 10%.

Topology	All	P+HF	Ghost	F_π
OS	10812	7380 ± 172	3432 ± 201	216 ± 44
SS	4400	2635 ± 104	1765 ± 123	138 ± 35

10 when of the same sign charge as the primary muon [10]. It is clear that a small fractions of ghost events contains a very large muon multiplicity. The contribution of fake muons is estimated assuming that the large majority of the tracks in a $\cos\theta \geq 0.8$ cone are pions. We correct the distribution in Fig. 21 (a) as follows. Given an event with n muons, we loop over all candidate tracks not associated to a muon stub and randomly generate fake muons using the probability that a pion mimics a muon signal. If m is the number of generated fake muons, we remove one event with $m+n$ muons in the distribution in Fig. 21 (a) and add one event to the bin with n muons. The fake subtraction reduces the number of $\cos\theta \geq 0.8$ cones that contain one or more additional muons from 40409 to 27539. The resulting distribution is shown in Fig. 21 (b). Appendix B describes a number of cross-checks which do not support the possibility that such a large number of muons contained in such a small angular cone is a detector artifact.

In conclusion, we are capable of predicting the number of additional muons in events in which the primary muons originate inside the beam pipe. In this case, the dominant sources of events are heavy flavor, Υ and Drell-Yan production, and most of the additional muons arise from sequential decays of single b quarks. At the same time, it seems difficult to account for the muon multiplicity distribution shown in Fig. 21 (b) if the ghost events were all due to ordinary sources, such as in-flight decays of pions and kaons, or hyperon decays in which the punchthrough of a hadronic prong mimics a muon signal. To summarize, we have uncovered two additional properties that differentiate ghost and P+HF events. A $\cos\theta \geq 0.8$ cone around the direction of a primary muon contains twice as many tracks as in P+HF events. These cones also contain a number of additional real muons that is approximately four times larger than in P+HF events.

[10] As examples, the 3rd bin indicates cones with 3 muons with charge $(+--)$ or $(-++)$; and the 21st bin indicates cones with 3 muons with charge $(+++)$ or $(---)$.

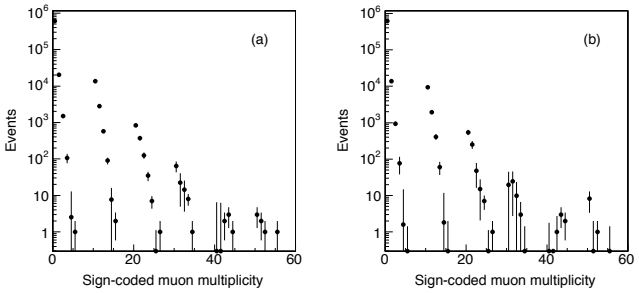

Fig. 21. Sign-coded multiplicity distribution of additional muons found in a $\cos\theta \geq 0.8$ cone around the direction of a primary muon in ghost events before (a) and after (b) correcting for the fake muon contribution. An additional muon increases the multiplicity by 1 when it has the opposite sign and by 10 when it has same sign charge as the primary muon. The background subtracted distribution is also listed in Table 10.

Table 10. Sign-coded, background subtracted, muon multiplicity in ghost events. Bins without entries are not shown. The multiplicity is not acceptance corrected because we do not know the mechanism producing ghost events. However, the detector acceptance for an additional muon with $p_T \geq 2$ GeV/c and $|\eta| \leq 1.1$ is 0.838±0.004. The detector acceptance for a primary muon with $p_T \geq 3$ GeV/c and $|\eta| \leq 0.7$ is 0.506 ± 0.003. The data correspond to an integrated luminosity of 1426 pb^{-1}.

Bin	Content	Bin	Content
0	620307 ± 3413	30	19.4 ± 25.6
1	13880 ± 573	31	24.2 ± 21.5
2	941 ± 135	32	9.8 ± 13.8
3	77 ± 39	33	3.0 ± 3.6
4	1.6 ± 13.2	34	0.00 ± 1.4
5	0.0 ± 1.4	40	-7.4 ± 9.2
10	9312 ± 425	41	-7.2 ± 7.0
11	1938 ± 173	42	1.0 ± 1.7
12	409 ± 71	43	3.0 ± 1.7
13	60 ± 23	44	2.0 ± 1.4
14	1.8 ± 10.1	50	8.1 ± 4.8
15	0.0 ± 2.0	51	0.0 ± 2.0
20	542 ± 91	52	1.0 ± 1.0
21	251 ± 61	55	0.0 ± 1.4
22	47 ± 31		
23	14.9 ± 12.8		
24	7.0 ± 3.0		
25	-3.1 ± 4.2		
26	1.0 ± 1.0		

7 Properties of additional muons in ghost events.

The request that primary muons originate in a decay region in which heavy flavor decays are exhausted selects a subset of events with a number of tracks and muons with $p_T \geq 2$ GeV/c much larger than that of P+HF processes. In the following, we investigate additional properties of this subsample, also referred to as multi-muon sample,

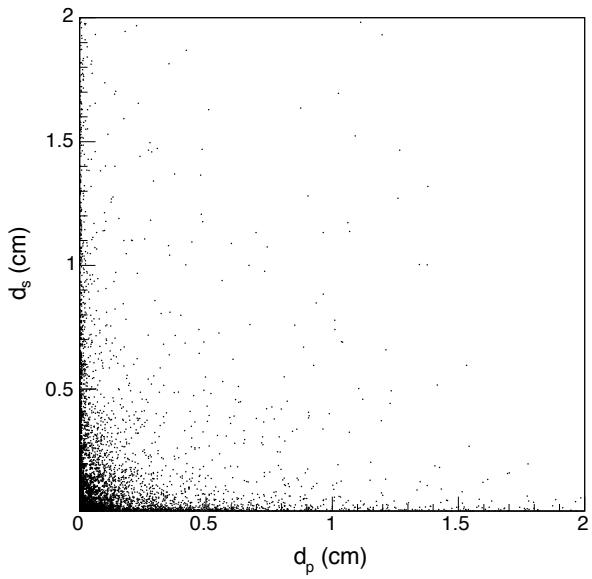

Fig. 22. Two-dimensional distribution of the impact parameter of additional muons, d_s, versus that of primary muons, d_p, for ghost events. Muons are selected with standard SVX requirements. The P+HF contribution has been removed.

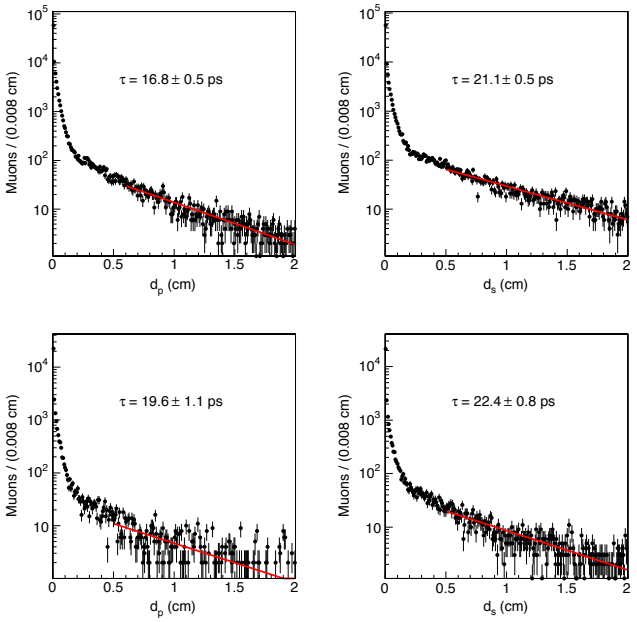

Fig. 23. Muon impact parameter distributions for events containing (top) only two muons or (bottom) more than two muons in a $\cos\theta \geq 0.8$ cone. We call d_p and d_s the impact parameter of primary and additional muons, respectively. The solid lines represent fits to the data distribution with an exponential function. The fit result is shown in each plot.

by selecting events that contain an increasing number of muons in a $\cos\theta \geq 0.8$ cone. This request enhances the contribution of this subset of ghost events and simultaneously suppresses the uncertain contribution of in-flight and hyperon decays and secondary interactions.

We first analyze the impact parameter distribution of additional muons in ghost events. Figure 22 shows the two-dimensional distribution of the impact parameter of primary muons versus that of all additional muons in a $\cos\theta \geq 0.8$ cone around its direction. The P+HF contribution has been removed using events in which the primary muons pass the tight SVX requirement. The impact parameter distribution of additional muons has the same shape of that of primary muons. However, the impact parameters of the additional and primary muons are loosely correlated (the correlation factor is $\rho_{d_p d_s} = 0.03$) [11].

Thus far, we have studied impact parameter distributions using muon tracks that pass the standard SVX selection in order to compare with previous experiments. For this study, we use muons without any SVX requirements, but select events containing two or at least three muons in a $\cos\theta \geq 0.8$ cone in order to enhance the well-understood heavy flavor contribution and suppress the uncertain contribution of in-flight and hyperon decays and secondary interactions. The corresponding impact parameter distributions are shown in Fig. 23. Fits with an exponential function to the impact parameter distributions of additional muons in the range $0.5 - 2.0$ cm, where no heavy flavor contribution is expected, return a slope of approximately 21.4 ± 0.5 ps. In contrast, fits to the impact parameters of primary muons yield slopes with appreciably smaller values. In the assumption that the exponential tail at large impact parameter is produced by the decay of long-lived objects, the difference is understood in terms of kinematic and trigger biases affecting the primary muons. As an example, Fig. 24 compares the result of fits to the impact parameter of fake primary muons and tracks corresponding to identified K^0_S decays. The fit to the track impact parameter yields a K^0_S lifetime in agreement with the PDG value of $\tau = 89.6$ ps. Because of the trigger bias, the lifetime measurement using fake primary muons yields a much smaller lifetime value.

In conclusion, the slope returned by the fits to the impact parameter tail of additional muons in ghost events is different from the lifetime of any known particle. If the impact parameter tails above 0.5 cm were produced by the decay of known particles - such as pions, kaons, K^0_S, and hyperons - the above described fits would have returned a slope at least as large as 90 ps.

The following cross-checks show that the impact parameter tail is not a detector effect that went unnoticed in the CDF t- and b-quark studies which customarily utilize muons and tracks with impact parameters smaller than $0.1 - 0.2$ cm. We study the impact parameter distributions of CMUP trigger muons accompanied by a $D^0 \to \pi^+ K^-$ (and charge-conjugate) candidates. We use events acquired with the μ-SVT trigger and reconstruct D^0 can-

[11] A correlation factor as large as 0.5 is expected if primary and additional muons originate from a common decay or secondary interaction vertex.

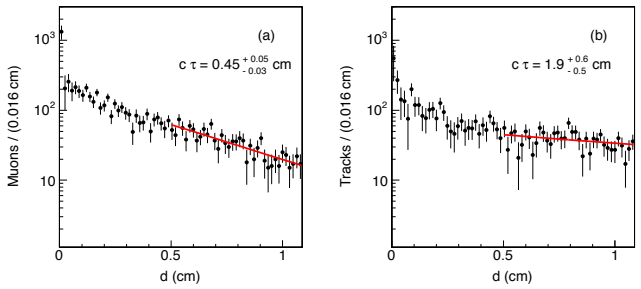

Fig. 24. Impact parameter distributions of (a) primary muons and (b) tracks of identified K^0_S decays. The combinatorial background under the K^0_S signal in Fig. 11 has been removed using a sideband subtraction method.

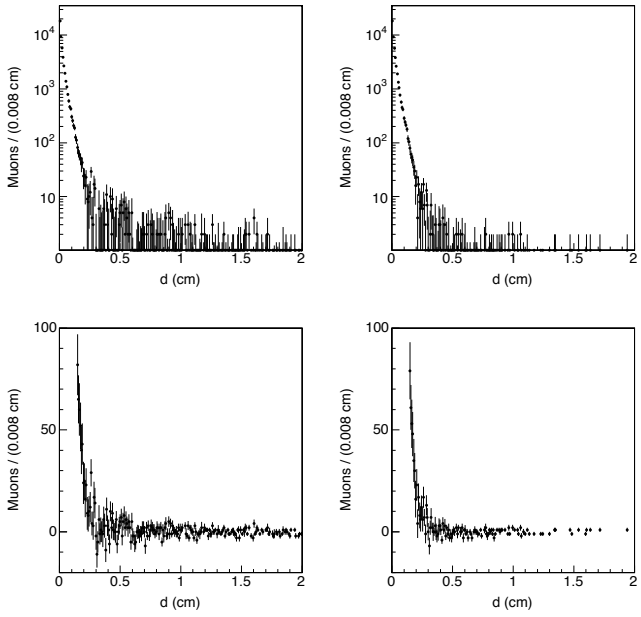

Fig. 25. Impact parameter distributions of CMUP muons which are accompanied by a D^0 meson and are selected without (left) SVX or with (right) standard SVX requirements. The bottom plots are magnified views to show distributions at large impact parameters. The contribution of the combinatorial background under the D^0 signal has been removed with a sideband subtraction method.

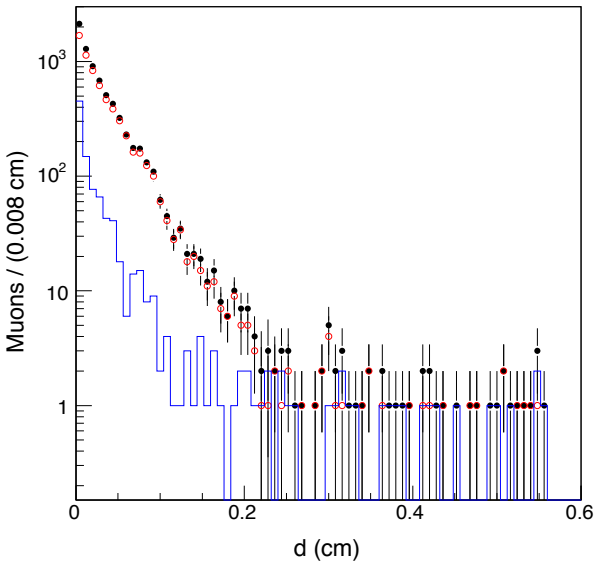

Fig. 26. Impact parameter distributions of muons accompanied by a D^0 meson and selected as the additional muons in this analysis. No SVX requirements are applied. All events (•) are compared to RS (○) and WS (histogram) combinations (see text). The contribution of the combinatorial background under the D^0 signal has been removed with a sideband subtraction method. The integral of the distributions above 0.35 cm is zero.

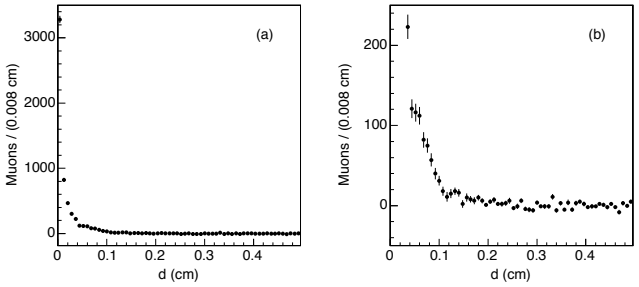

Fig. 27. Impact parameter distribution of (a) additional muons found in events in which the primary muons are selected with tight SVX requirements. The same distribution is plotted in (b) with a magnified vertical scale. Additional muons are selected without SVX requirements. The fake muon background has been subtracted.

didates by attributing the kaon mass to the track with the same charge as the muon (RS combinations as expected for $\mu + D^0$ systems produced by b hadron decays). We retain combinations in which the muon plus two-track system has an invariant mass smaller than 5 GeV/c^2. As expected since fake CMUP muons are negligible, no wrong-sign (WS) combinations are found. The impact parameter distribution of CMUP muons produced by B decays, shown in Fig. 25, is exhausted above 0.5 cm.

Figure 26 shows the analogous plot for muons selected as the additional muons in this analysis ($p_T \geq 2$ GeV/c and $|\eta| \leq 1.1$) in events triggered by a D^0 candidate. No high impact parameter tails are observed. The fraction of fake muons, measured as the number of WS combinations, is approximately 2% and well predicted by our parametrized fake muon probability per track.

The tail of the impact parameter distribution of additional real muons in events in which the primary muons pass the tight SVX selection, shown in Fig. 27, also does not extend beyond 0.5 cm.

7.1 Lifetime

The fact that multi-muon events have been isolated by the request that at least one of the trigger muons originates beyond the beam pipe as well as the shape of the impact parameter distribution of additional muons suggest that they could be produced by objects with lifetime longer than that of b quarks. In the previous section, we have estimated this hypothetical lifetime by using a small fraction of events in the tail of the muon impact parameter distribution. In the following, we search for a confirmation based on the entire sample of ghost data. We have seen in the previous section that the impact parameters of muons contained in the same cone are not strongly correlated. This would happen if each muon arises from the decay of a different object. Therefore, we search for secondary vertices produced by pairs of tracks with $p_T \geq 1$ GeV/c and opposite charge contained in a 36.8° cone around the direction of each primary muon. Track pairs are constrained to arise from a common space point. Combinations are discarded if the three-dimensional vertex fit returns a χ^2 larger than 10. If a track is associated with more than one secondary vertex, we discard those with lower fit probability. For each secondary vertex, we define L_{xy} as the distance between the secondary and primary event vertices projected onto the transverse momentum of the two-track system. Combinations of tracks arising from the primary vertex or from the decay of different objects yield a L_{xy} distribution symmetric around $L_{xy} = 0$. An excess at positive L_{xy} is a property of the decay of a long-lived object.

We use $K^0_S \to \pi^+\pi^-$ decays to verify with data the detector response in the impact parameter region populated by ghost events. We search for K^0_S decays in the dimuon dataset used for this analysis by pairing tracks of opposite charge with $p_T \geq 0.5$ GeV/c, $|\eta| \leq 1.1$, and opening angle smaller than 60°. Track combinations are constrained to arise from a common space point. Combinations are discarded if the three-dimensional vertex fit returns a χ^2 larger than 10 or the L_{xy} distance is smaller than 0.1 cm. In this case, the L_{xy} distance is also corrected for the Lorentz boost of the two-track system. Figure 28 (a) shows the invariant mass spectrum of the two-track systems passing this selection. The combinatorial background under the K^0_s signal, integrated from 0.486 to 0.510 GeV/c^2, is removed by subtracting the events contained in the side bands 0.474 − 0.486 and 0.510 − 0.522 GeV/c^2. The background subtracted L_{xy} distribution, shown in Fig. 28 (b), is consistent with the K^0_S lifetime of 89.5 ps [5].

Figure 29 shows the difference between the positive and negative L_{xy} distributions of secondary vertices reconstructed in P+HF and ghost events. The L_{xy} distribution for P+HF events is dominated by partially reconstructed decays of b and c hadrons and decreases by approximately three orders of magnitude in the first centimeter [12]. The shape of the distribution for ghost events, when compared to that for heavy flavors and K^0_S decays, is not inconsistent with the hypothesis that a small but significant fraction of ghost events arise from the production and decay of objects with a lifetime longer than that of b hadrons and shorter than that of K^0_S mesons.

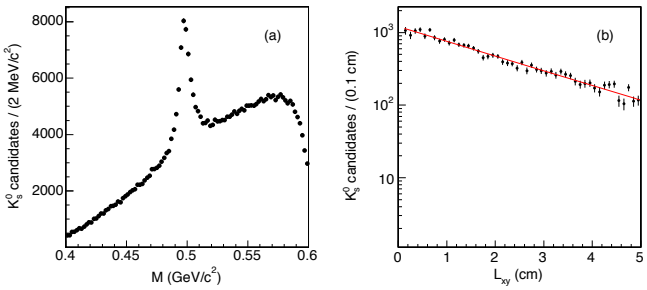

Fig. 28. Invariant mass distribution (a) of $K^0_S \to \pi^+\pi^-$ candidates. The background subtracted L_{xy} distribution of K^0_S mesons (b) is compared to the expectation based on the K^0_S measured lifetime [5].

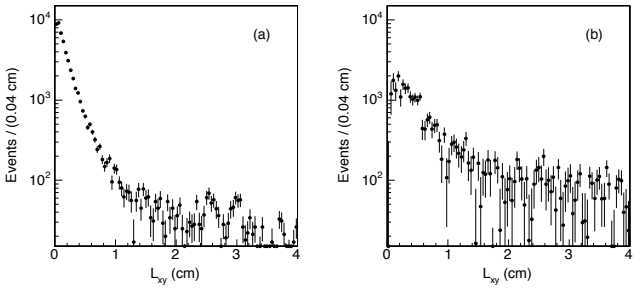

Fig. 29. Distribution of the distance L_{xy} of reconstructed secondary vertices due to long-lived decays in (a) P+HF and (b) ghost events. The combinatorial background has been removed by subtracting the corresponding negative L_{xy} distributions. The data correspond to an integrated luminosity of 742 pb^{-1}.

7.2 Track multiplicity

As discussed in Sec. 6, ghost events include a sizable contribution from ordinary sources such as in-flight-decays, and K^0_S and hyperon decays. The average track multiplicity in ghost events is a factor of two larger than in P+HF events. In order to study the average multiplicity of multi-muon events, we use events that contain at least three muons in a 36.8° cone. Figure 30 shows the average number of all tracks with $p_T \geq 2$ GeV/c contained in a 36.8° cone around a primary muon as a function of the total transverse momentum of the tracks.

[12] The distribution above 1.2 cm which includes small bumps at 2.5 and 3.0 cm is due to secondary interactions of hadronic tracks in the detector material. The position of the detector material is smeared with respect to that in Fig 14 because measured with respect to the primary event vertex rather than the nominal beamline and projected onto the momentum vector carried by the tracks.

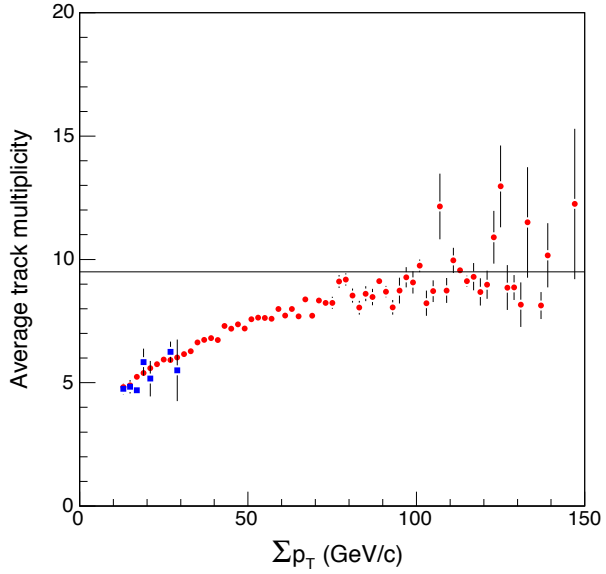

Fig. 30. Average number of tracks in a 36.8° cone around the direction of a primary muon as a function of $\sum p_T$, the transverse momentum carried by all the tracks. We use cones containing at least three muons. Data (•) are compared to the P+HF expectation (■) based on the few events predicted by the heavy flavor simulation, scaled to reproduce the measured heavy-flavor cross sections and implemented with the probability that hadronic tracks mimic a muon signal. The reconstruction efficiency for these tracks is close to unity.

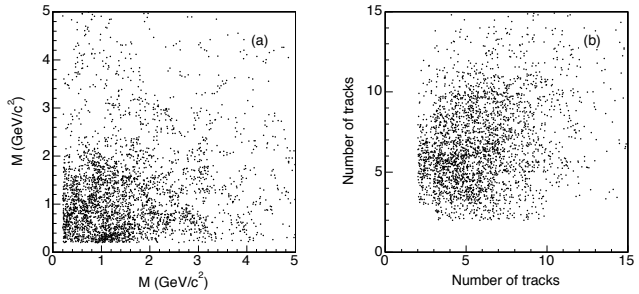

Fig. 31. Two-dimensional distributions of (a) the invariant mass, M, of all muons and (b) the total number of tracks contained in a 36.8° cone when both cones contain at least two muons. The P+HF and fake muon contributions have been subtracted.

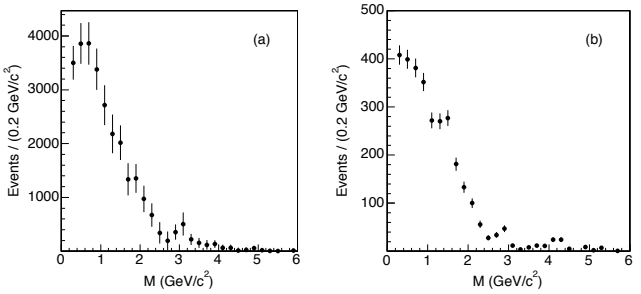

Fig. 32. Distributions of invariant mass, M, of all muons contained in (a) the 27990 36.8° cones with two or more muons and (b) in each cone of the 3016 events in which both cones contain two or more muons. The P+HF and fake muon contributions have been subtracted.

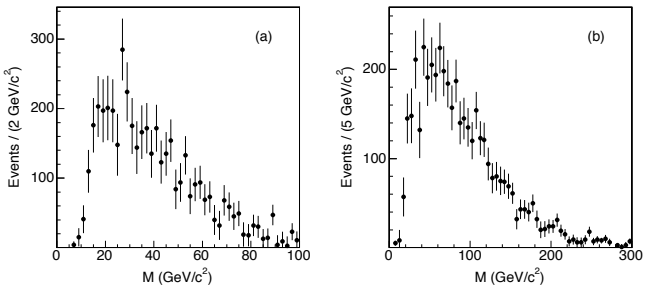

Fig. 33. Invariant mass distribution of (a) all muons and (b) all tracks for events in which both cones contain at least two muons. The P+HF and fake muon contributions are subtracted. The data correspond to an integrated luminosity of 2100 pb^{-1}.

7.3 Cone correlations

In the previous section, we have investigated the kinematics and topology of muons and tracks contained in a single 36.8° cone around the direction of a primary muon. In this section, we extend the investigation to the rate and properties of events in which two 36.8° cones contain a muon multiplicity larger than that of P+HF events. After subtracting the P+HF and fake muon contribution, in ghost events there are 27990 ± 761 cones that contain two or more muons, 4133 ± 263 cones that contain three or more muons, and 3016 ± 60 events in which both cones contain two or more muons. It follows that approximately 13% of the ghost events in which one cone contains two or more muons also contain a second cone with the same feature.

The following distributions serve the purpose of showing that, when a second cone containing multi muons is found, it has the same characteristics of the first found multi-muon cone. Figure 31 plots two-dimensional distributions of the invariant mass of all muons and of the number of tracks with $p_T \geq 2$ GeV/c contained in each cone for the 3016 events containing two cones with two or more muons. Figure 32 shows that the invariant mass distribution of all muons contained in the 27990 cones containing at least two muons is consistent with that of the 3016 events in which both cones contain at least two muons. Figure 33 shows the invariant mass distribution of all muons and all tracks with $p_T \geq 2$ GeV/c in events in which both cones contain two or more muons.

8 Conclusions

We have studied a sample of events containing at least two central muons with $p_T \geq 3$ GeV/c and invariant mass $5 \leq m_{\mu\mu} \leq 80$ GeV/c^2. The data sets were collected with the CDF II detector at the Fermilab Tevatron collider, and correspond to integrated luminosities up to 2100 pb^{-1}. Similar data samples have been previously used by the CDF and DØ collaborations to derive measurements of the correlated $\sigma_{b\to\mu,\bar{b}\to\mu}$ cross section that are inconsistent with the NLO theoretical prediction. A similar data set was also used by the CDF collaboration to extract a value of $\bar{\chi}$, the average time-integrated mixing probability of b-flavored hadrons, that is appreciably larger than that reported by the LEP experiments. This analysis extends a recent study [6] by the CDF collaboration which has used a dimuon data sample to re-measure the correlated $\sigma_{b\to\mu,\bar{b}\to\mu}$ cross section. Following tradition, the value of $\sigma_{b\to\mu,\bar{b}\to\mu}$ is measured using the sample composition as determined by fitting the impact parameter distribution of these primary muons with the expected shapes from all sources deemed significant: semileptonic heavy flavor decays, prompt quarkonia decays, Drell-Yan production, and instrumental backgrounds from prompt hadrons or hadrons from heavy-flavor decays that mimick the muon signal (the sum of these sources is referred to as P+HF contribution). Reference [6] reports $\sigma_{b\to\mu,\bar{b}\to\mu} = 1549\pm133$ pb for muons with $p_T \geq 3$ GeV/c and $|\eta| \leq 0.7$. That result is in good agreement with the NLO prediction as well as with analogous measurements that identify b quarks via secondary vertex identification [26,27]. The study in Ref. [6] uses a subset of dimuon events in which each muon track is reconstructed in the SVX with hits in the two inner layers and in at least four of the inner six layers. These tight SVX requirements select events in which both muons originate within 1.5 cm from the nominal beam line. According to the simulation, approximately 96% of the dimuon events contributed by known P+HF processes satisfy this condition. By varying the SVX selection requirements, this study identifies the presence of a previously ignored contribution to the dimuon triggered sample, referred to as ghost events, that fails this condition. The relative size of the ghost contribution depends on the type of SVX requirements applied to the trigger muons. As SVX requirements select trigger muons produced closer to the beamline, the size of the ghost contribution is reduced in comparison to that of the P+HF components that are not strongly affected by this requirement. The ghost component was present in previous $\sigma_{b\to\mu,\bar{b}\to\mu}$ [7,8] and $\bar{\chi}$ [4] measurements in which this strict decay-radius requirement was not made. The magnitude of the ghost contribution is comparable to the $b\bar{b}$ contribution when no SVX selection is made and in combination would account for the measurement reported in [8]. When using SVX requirements similar to those of previous analyses, the magnitude of the ghost contribution (72553 ± 7264 events, equally split in OS and SS dimuons), when added to the $b\bar{b}$ contribution of 194976 ± 10221 events [6], coincides with the cross section measurement reported in [7] and the $\bar{\chi}$ value reported in [4]. Finally, the ghost sample is shown to be the source of the dilepton invariant mass discrepancy reported in Ref. [3]. When applying the tight SVX criteria to primary muons, the rate and kinematic of additional muon in the events is well described by known P+HF sources and is dominated by sequential semileptonic heavy flavor decays. In contrast, without any SVX requirement the invariant mass spectrum of primary and additional muon pairs is not well modeled by the P+HF simulation and the inconsistencies at low invariant mass reported in Ref. [3] are reproduced. Our study shows that ghost events offer a plausible resolution to these long-standing inconsistencies related to $b\bar{b}$ production and decay. The observed rate of ghost events is consistent with what expected from in-flight-decays of pions and kaons or punchthrough of hadronic prongs of K^0_S and hyperon decays. However, a small but significant fraction of these events has features that cannot be explained in terms of known sources with our present understanding of the CDF II detector, trigger and event reconstruction. The nature of these events is characterized by the following properties. The average number of tracks contained in a 36.8° cone around the direction of each primary muon is two times larger than that of P+HF events. After subtracting the contribution of hadrons mimicking a muon signal, 36.8° cones contain a rate of muon candidates that is approximately four times larger than that due to sequential semileptonic decays of b quarks. In contrast with sequential semileptonic decays of b hadrons, primary and additional muon candidates have same or opposite charge with equal probability. The impact parameter distribution of additional muon candidates, as well as that of displaced secondary vertices reconstructed using pairs of tracks of opposite charge contained in 36.8° cones, have shapes different from what is expected if they were produced by known long-lived particles.

9 Acknowledgments

We thank the Fermilab staff and the technical staffs of the participating institutions for their vital contributions. This work was supported by the U.S. Department of Energy and National Science Foundation; the Italian Istituto Nazionale di Fisica Nucleare; the Ministry of Education, Culture, Sports, Science and Technology of Japan; the National Science Council of the Republic of China; the Swiss National Science Foundation; the A.P. Sloan Foundation; the Korean Science and Engineering Foundation and the Korean Research Foundation; the Science and Technology Facilities Council and the Royal Society, UK; the Institut National de Physique Nucleaire et Physique des Particules/CNRS; the Russian Foundation for Basic Research; the Ministerio de Ciencia e Innovación, Spain; the European Community's Human Potential Programme; the Slovak R&D Agency; and the Academy of Finland.

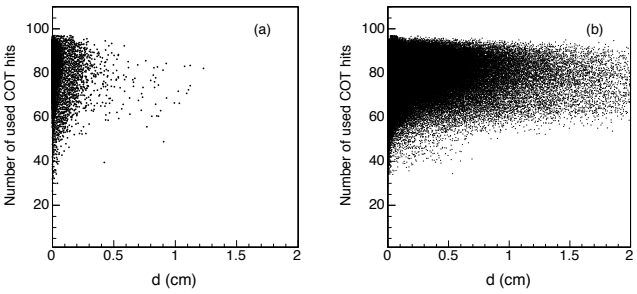

Fig. 34. Number of COT hits associated with primary muon tracks as a function of the track impact parameter for (a) P+HF and (b) ghost events.

A Detector level distributions in P+HF and ghost events

This appendix presents a few of many detector-level distributions that have been investigated looking for pathologies in track reconstruction, muon reconstruction, detector response, and in the observed properties of the ghost events. The assumption is that detector and pattern recognition failures are not an issue if detector-level distributions for ghost events are similar to those for P+HF events, which in turn are correctly modeled by a simulation based on the HERWIG and GEANT Monte Carlo programs.

A.1 Quality of reconstructed tracks

A visual investigation of the display of reconstructed muon tracks and associated COT and SVX hits has not shown any indication of detector or track-reconstruction program failures. COT tracks reconstructed using hits in at least 20 COT layers are considered well measured tracks and are used in most CDF analyses. Figure 34 shows the number of COT hits used to reconstruct primary muon tracks as a function of the track impact parameter. In both P+HF and ghost events, muon tracks are associated with an average of 75 hits, and the average number of associated hits does not depend on the impact parameter value.

As also shown by cosmic muons in Fig. 2 (b), the impact parameter of COT tracks associated with at least three silicon hits is measured with a rms resolution of approximately 30 μm [6]. We have studied the impact parameter resolution of COT tracks without silicon hits, which populate ghost but not P+HF events, by using muons from Υ decays included in our data sample. The impact parameter distribution is shown in Fig. 35. The rms resolution is approximately 230 μm, and the impact parameter distribution is exhausted beyond 0.15 cm. Therefore, the large impact parameter tail characteristic of muons in ghost events is not due to tracks reconstructed without silicon hits.

We have studied a large sample of K^0_S mesons reconstructed in the dimuon sample by using COT tracks with and without silicon hits, and with small or very large impact parameters (see Fig. 28). The observed L_{xy} distribution is correctly modeled by the value of the K^0_S lifetime [5]. As shown in Figs. 4, 25, and 26, primary muons in ghost events are not accompanied by D^0 mesons and muons in events triggered by the request of a D^0 meson do not exhibit any large impact parameter tail. It is therefore unlikely that a significant fraction of ghost events arises from detector or pattern recognition failures in standard P+HF events.

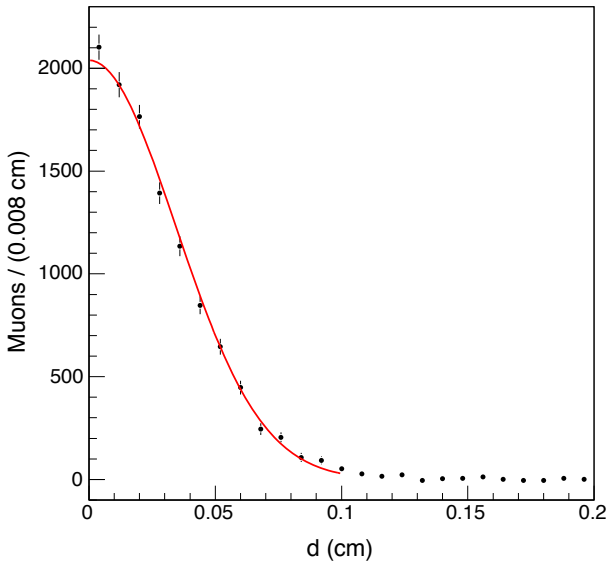

Fig. 35. Impact parameter distribution of tracks corresponding to muons from Υ decays. Tracks are not associated with silicon hits. The combinatorial background under the Υ signal has been removed with a sideband subtraction technique. The solid line is a fit to the data with a Gaussian function.

A.2 Quality of reconstructed muons

A track is accepted as a muon if the $r-\phi$ distance between its projection onto a muon detector and a muon stub is $\Delta x \leq 30$, 40, and 30 cm for the CMU, CMP, and CMX detector, respectively. For CMX or CMU muons, we also construct the quantity $\chi^2 = (\Delta x/\sigma)^2$, where σ is a rms deviation that includes the effect of muon multiple scattering and energy loss. These quantities are compared in Figs. 36 and 37 for primary and additional muons in P+HF and ghost events. Table 11 shows the fraction of additional muons identified by the different detectors in P+HF and ghost events. These matching distributions, as well as the fractional usage of different muon detectors, in ghost events are not significantly different to those of P+HF events. Since we are able to predict the rate of additional muons in P+HF events, the response of the muon detector is an unlikely candidate to explain the large excess of additional muons in ghost events.

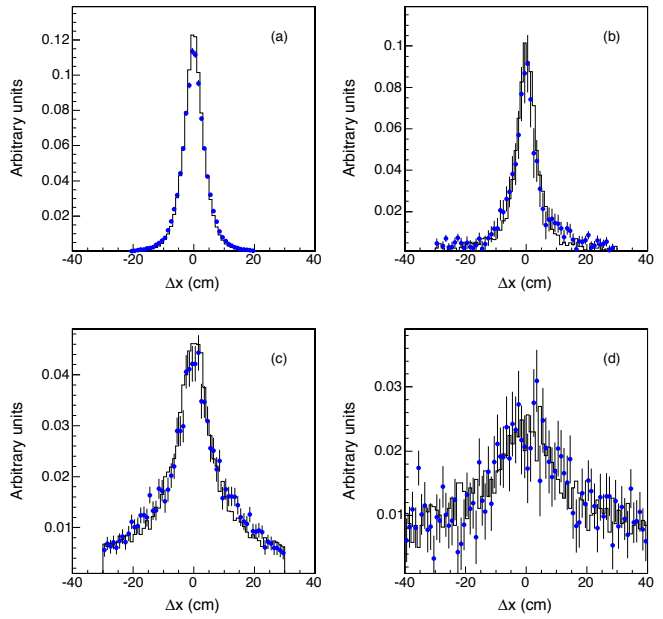

Fig. 36. Distributions of Δx (see text) for (a) primary and (b) additional CMUP muons, and additional (c) CMU or (d) CMP muons in P+HF (histogram) and ghost (•) events.

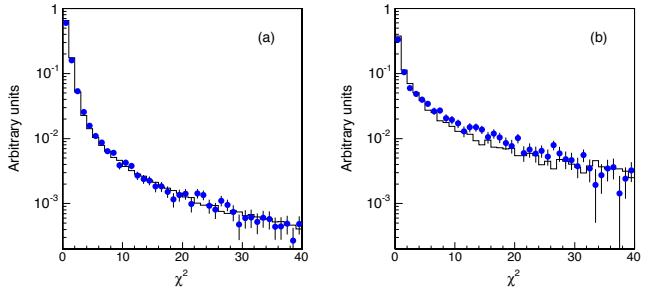

Fig. 37. Distributions of χ^2 (see text) for (a) primary and (b) additional muons in P+HF (histogram) and ghost(•) events.

Table 11. Fractional contributions (%) to additional muons of different detectors in P+HF and ghost events.

Sample	CMUP	CMU	CMP	CMX
P+HF	17.0 ± 0.4	53.0 ± 0.7	26.0 ± 0.5	4.0 ± 0.2
Ghost	14.0 ± 0.8	60.0 ± 1.4	24 ± 1	2.0 ± 0.4

The Δx distributions for CMU and CMP muons in Fig. 36 show a significant quasi-flat contribution due to random track-stub matches under the Gaussian signal of real muons. This contribution is negligible for CMUP muons. These features are consistent with the fake muon prediction based on the fake probability per track derived using the decay products of D^0 mesons.

For CMUP muons, the fake probability has been verified using the data in Ref. [6]. Ref. [6] estimates the fraction of dimuons due to heavy flavor production that are faked by hadrons from heavy flavor decays in two complementary ways. This fraction is estimated by applying the fake probability per track to simulated hadrons from heavy flavor decays. This fraction is also estimated by simultaneously fitting the impact parameter distributions of dimuon events selected with standard and tight χ^2 requirements, and therefore containing different fractions of fake muons. The fit result shows that the fraction of fake muons is negligible, and slightly overestimated by the fake probability prediction. This conclusion is also supported by the fact that, when using primary CMUP muons no wrong-sign μD^0 candidates are observed in Fig. 4. The fit to the muon impact parameters in Ref. [6] yields the rate of dimuons due to $b\bar{b}$ and bg production (BB and BP component in Table 1, respectively). In the latter case, the muon signal is mimicked by a prompt hadron in the gluon jet. The ratio of these components returned by the fit is 0.194 ± 0.013. When applying the fake probability per track to simulated bg events normalized to the observed $b\bar{b}$ cross section, Ref. [6] predicts this ratio to be 0.21 ± 0.01. These comparisons show that the fake CMUP probability per track cannot be underestimated by more than 10%. Since the rate of fake CMUP muons predicted in Table 9 is approximately 4% of the signal, it seems unlikely that the additional CMUP signal in ghost events can be explained by an underestimate of the fake rate. In turn, this supports the main findings of our study that uses all muon detectors since they are consistent with the result based on CMUP muons only.

B Robustness of the fake muon prediction

In this appendix, we discuss the possibility that large numbers of muons detected in small angular cones might be a detector artifact. The display of the muon chamber hits in events that contain four or more muons does not yield any indication of a detector malfunction. However, there are events in which certain areas of the muon detectors have a dense clustering of dozens of hits. In these events, some muons correspond to tracks linked to muon stubs constructed in those clusters. This raises a concern that the fake rate in multi-muon events in which hadronic tracks can take advantage of hits in the muon chambers produced by real muons or by hadronic punchthrough might be underestimated.

Traditionally, CDF analyses that search for soft ($p_T \geq 2$ GeV/c) muons estimate the fake contribution by applying to all candidate tracks a parametrized probability of penetrating the calorimeter and mimicking a muon signal that does not depend on the event characteristics [25]. This probability per track is measured using pions and kaons from D^0 decays. After requiring that D^0 candidates have an appreciable proper decay time in order to select D^0 mesons from b-hadron decays, the b jet defined by a 36.8° cone around the D^0 direction contains an average of 0.02 muons and 1.6 additional tracks with $p_T \geq 2$ GeV/c. The muon fake probability does not increase at all when using D^0 prongs accompanied by at least two tracks.

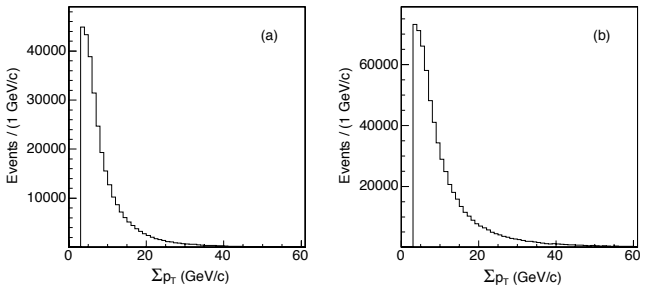

Fig. 38. Distribution of the transverse momentum carried by all tracks with $p_T \geq 1$ GeV/c contained in a 36.8° cone around a primary muon in (a) P+HF and (b) ghost events.

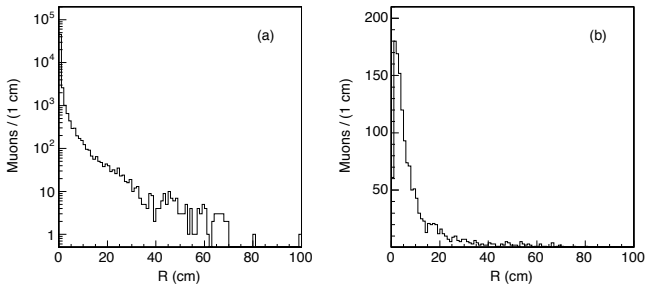

Fig. 39. Distributions of R, the distance of dimuon vertices from the nominal beam line for primary muons with impact parameter (a) smaller and (b) larger than 0.3 cm.

Unfortunately, the track multiplicity of multi-muon events is larger than that of b jets and we do not possess an understood control sample of data with a number of tracks and muons as large as in ghost events that could be used to verify the fake muon estimate. In the following, we list a number of indirect tests and comparisons with P+HF events that should have flagged this type of problem if it existed.

The excess of muons in ghost events cannot simply arise from a breakdown of the method used to predict the fake rate when applied to high E_T jets with many tracks that are not contained in the calorimeter and muon absorber. This effect was not observed in previous analyses. We would also have found multi-muons events in the P+HF contribution because, as shown in Fig. 38, the distributions of the transverse momentum carried by all tracks with $p_T \geq 1$ GeV/c and contained in a 36.8° cone in ghost and P+HF events are quite similar.

In Sec. 6, we have searched for additional muons using the CMUP detector only. Because of the larger number of interaction lengths traversed by hadronic tracks, the fake muon contribution is negligible and has been verified with the data [6]. This method yields results which are consistent with the standard method.

In the standard method, a track is identified as a muon if the distance of its projection onto a muon detector from a muon stub is $\Delta x \leq 30$, 40, and 30 cm for the CMU, CMP, and CMX detector, respectively. For CMX or CMU muons with $p_T = 2$ GeV/c, these Δx cuts correspond to the requirement that the track extrapolation and the muon stub match within 3 σ in the $r-\phi$ plane, where σ is a rms deviation that includes the effect of multiple scattering and energy loss. We have selected additional muons with the increasingly stricter requirements that track-stub matches are within 3 and 2 σ, respectively. The latter requirement reduces the number of multiple-muon combinations by a factor of two, but does not affect the salient features of the multiplicity distribution in Fig. 21 (a).

We have compared Δx and σ distributions of muon-track matches for the different muon detectors in P+HF and ghost events (see Appendix A). These distributions, as well as the fractional usage of different muon detectors, in ghost events are not significantly different to those of P+HF events in which the fake rate is correctly understood. Since the CMUP detector has a negligible and verified fake contribution, an anomalous increase of the fake rate with respect to P+HF events should have dramatically changed the relative occupancy of the different muon detectors as well as the shape of the matching distributions.

To investigate if the fake probability per track increases in events in which a track has penetrated the calorimeter, we have studied the rate of additional muon in events triggered by the punchthrough of a K_S^0 prong. As shown at the beginning of Sec. 5, we have identified 5348 ± 225 K_S^0 candidates in the dimuon data, and 96 ± 41 of them contain at least an additional muon in the event. By applying the fake muon probability to all candidate tracks in the events with a K_S^0 candidate, we predict 86 ± 30 events with at least an additional fake muon, consistent with the observation.

The appearance of multi-muon events is correlated to the presence of muons with large impact parameters. As discussed earlier, inelastic secondary interactions inside the tracking detector do not contribute significantly to the total number of ghost events. This does not exclude the possibility that the smaller number of multi-muon ghost events are due to secondary interactions that point into calorimeter cracks. We search for secondary interactions by combining primary muons with small and large impact parameters with all additional muons in a 36.8° cone around the muon direction. Dimuon combinations are constrained to arise from a common space point. They are discarded if the three-dimensional vertex fit returns a χ^2 larger than 10. The distribution of R, the distance of a reconstructed secondary vertex from the detector origin in the plane transverse to the beam line, is shown in Fig. 39 for primary muons with small and large impact parameters. The absence of spikes in the distributions does not support the hypothesis. In addition, if this type of secondary interaction were the source of multi-muon events, the impact parameters of the different muons would have beeen highly correlated.

References

1. M. L. Mangano, P. Nason, and G. Ridolfi, Nucl. Phys. **B373**, 295 (1992).
2. F. Happacher *et al.,* Phys. Rev. D **73**, 014026 (2006); F. Happacher, *Status of the Observed and Predicted $b\bar{b}$ Cross Section at the Tevatron*, Proceedings of Tsukuba 2006, Deep inelastic scattering, edited by M. Kuze, K. Nagano, K. Tokushuku, World Scientific, 645 (2007).
3. G. Apollinari *et al.,* Phys. Rev. D **72**, 072002 (2005).
4. D. Acosta *et al.,* Phys. Rev. D **69**, 012002 (2004).
5. W.-M. Yao *et al.,* J. Phys. G **33**, 1 (2006).
6. T. Aaltonen *et al.,* Phys. Rev. D **77**, 072004 (2008).
7. F. Abe *et al.,* Phys. Rev. D **55**, 2546 (1997).
8. B. Abbott *et al.,* Phys. Lett. B **487**, 264 (2000).
9. F. Abe *et al.,* Nucl. Instrum. Methods Phys. Res., Sect. A **271**, 387 (1988).
10. R. Blair *et al.,* Fermilab Report No. FERMILAB-Pub-96/390-E (1996).
11. C. S. Hill *et al.,* Nucl. Instrum. Methods Phys. Res., Sect. A **530**, 1 (2004).
12. A. Sill *et al.,* Nucl. Instrum. Methods Phys. Res., Sect. A **447**, 1 (2000).
13. T. Affolder *et al.,* Nucl. Instrum. Methods. Phys. Res., Sect. A **453**, 84 (2000).
14. T. Affolder *et al.,* Nucl. Instrum. Methods Phys. Res., Sect. A **526**, 249 (2004).
15. G. Ascoli *et al.,* Nucl. Instrum. Methods Phys. Res., Sect. A **268**, 33 (1988).
16. J. Elias *et al.,* Nucl. Instrum. Methods. Phys. Res., Sect. A **441**, 366 (2000).
17. D. Acosta *et al.,* Nucl. Instrum. Methods Phys. Res., Sect. A **461**, 540 (2001).
18. R. Downing *et al.,* Nucl. Instrum. Methods Phys. Res., Sect. A **570**, 36 (2007).
19. M. M. Block and R. N. Cahn, Rev. Mod. Phys. **57**, 563 (1985).
20. S. Klimenko *et al.,* Fermilab Report No. FERMILAB-FN-0741 (2003).
21. B. Ashmanskas *et al.,* Nucl. Instrum. Methods Phys. Res., Sect. A **518**, 532 (2004).
22. G. Marchesini and B. R. Webber, Nucl. Phys. B **310**, 461 (1988); G. Marchesini *et al.,* Comput. Phys. Commun. **67**, 465 (1992).
23. D. J. Lange, Nucl. Instrum. Meth. A **462**, 152 (2001). We use version V00-14-05 downloaded from `http://www.slac.stanford.edu/BFROOT/dist/packages/EvtGen/`.
24. R. Brun *et al.,* CERN Report No. CERN-DD-78-2-REV; R. Brun *et al.,* CERN Programming Library Long Write-up W5013 (1993).
25. F. Abe *et al.,* Phys. Rev. D **50**, 2966 (1994); T. Affolder *et al.,* Phys. Rev. D **64**, 032002 (2001); D. Acosta *et al.,* Phys. Rev. D **72**, 032002 (2005).
26. D. Acosta *et al.,* Phys. Rev. D **69**, 072004 (2004).
27. T. Shears, *Charm and Beauty Production at the Tevatron*, Proceedings of the Int. Europhys. Conf. on High Energy Phys., PoS (HEP2005), 072 (2005).
28. A. Goshaw *et al.,* Phys. Rev. Lett **34**, 607 (1975).
29. F. Abe *et al.,* Phys. Rev. Lett. **64**, 157 (1990).